(4)

# ISTITUTO NAZIONALE DI FISICA NUCLEARE

**Sezione di Milano**

---

**INFN/AE-92/09**
**27 Febbraio 1992**

G. Ranucci, R. Cavalletti, P. Inzani, S. Schönert:

## PERFORMANCES OF LARGE CATHODE AREA PHOTOTUBES FOR UNDERGROUND PHYSICS APPLICATIONS

**Servizio Documentazione**
dei Laboratori Nazionali di Frascati

**INFN - ISTITUTO NAZIONALE DI FISICA NUCLEARE**
Sezione di Milano

**INFN/AE-92/09**
**27 Febbraio 1992**

# PERFORMANCES OF LARGE CATHODE AREA PHOTOTUBES FOR UNDERGROUND PHYSICS APPLICATIONS

*G. Ranucci, R. Cavaletti, P. Inzani*
*Istituto Nazionale di Fisica Nucleare, via Celoria 16 - 20133 Milano, Italy*

*S. Schönert*
*Technical University of Munich, D-8046 Garching, Germany*

## ABSTRACT

In this report we describe the main results of the test activity performed on the large cathode area phototubes Burle C83061E, Hamamatsu R4558, Philips XP1802 and Thorn Emi 9351. These devices, developed both for large-scale Cerenkov detectors and for Solar Neutrino detectors, have been considered as potential candidates for the use in the proposed low energy solar neutrino experiment Borexino. Thus the measurements carried out have been particularly focused to evaluate the parameters of these photomultipliers more critically affecting the overall physics performances of the detector.

## 1. - INTRODUCTION

In the frame of the R&D activity carried out for the proposed solar neutrino experiment Borexino (1), to be installed in the Gran Sasso Laboratory, a thorough evaluation has been performed of the performances of several large photocathode area tubes available on the market, in order to identify the one best suited for the use in the detector. The selection has been performed essentially evaluating the impact of the main technical features of the candidate tubes on the overall detector performances. For this purpose the principal characteristics of the tubes were thoroughly analyzed in conjuction with the detector operation, and then divided into two categories, the former including those less crucial for the success of the experiment, the latter those considered vital for the achievement of the physics goals of Borexino. By comparing the values of the technical characteristics of the four tubes, differently weighted according to their belonging to the low or high priority class of parameters, it was possible to identify the one whose features were the best trade-off in view of the requirements of Borexino. The PMT's taken into account were: the Hamamatsu 20" tubes: R1449, R3600 and R1449Z; the 10.4" Burle C83061E; the 9" Philips XP1802; the 8" Thorn Emi 9351 and Hamamatsu R4558. Among these devices the 8" Thorn Emi 9351 tube has been identified as the best for the operation in the Borexino detector.

## 2. - GUIDELINE PARAMETERS ADOPTED FOR THE TUBE SELECTION

### 2.1. - Low priority parameters

1) Maximum achievable gain

The maximum gain determines the degree of flexibility achievable in the experimental operation to properly adjust the overall detector sensitivity and to optimize its performances.

2) Gain vs. high voltage

The functional relation between the applied high voltage and the resulting gain, even if fluctuating from tube to tube, is useful to identify broadly the range of voltages needed to operate the photomultipliers at a gain presently supposed to be initially fixed at about $10^7$. In addition, since too high applied voltages can produce unwanted effects in the tube (usually related as field effects) it is important that a proper gain could be achieved at reasonable low voltage value (less than 2000 V).

3) Anode pulse rise time, fall time and fwhm

These characteristics, practically describing the time shape of the anode pulse, have some impact on the trigger system. Indeed a fast, narrow pulse, with limited rise time (around 2 o 3 ns) is well suited for a fast responding trigger electronics, to produce a precisely timed trigger signal.

4) Photocathode and anode uniformity

These characteristics reflect the degree of accuracy in the deposit of the photocathode layer and in the design of the input optic stage. They are thus a valuable indication of the quality of the phototube.

5) Maximum non destructing vibration level

The maximum sinusoidal vibration level (at 15 Hz) the tube can withstand is important for an experiment whose expected lifetime is of the order of several years.

2.2. - High priority parameters

1) Photocathode quantum efficiency

The quantum efficiency is the probability of a photoelectron to be emitted upon the incidence of one photon on the cathode. Since it determines, together with the effective area coverage, the number of detected photoelectrons per MeV of energy deposit in the scintillator, it is crucial in assessing the spatial resolution, the time resolution and the signal threshold.

Hence the higher this parameter, the better the overall experimental features of Borexino.

It must be pointed out that the manufacturers were esplicitely requested for a specification at 420 nm, since the scintillation light is sharply peaked at this wavelength.

2) Single photoelectron transit time spread

This parameter influences the definition of the fiducial volume and determines the precision of the vertex reconstruction.

The maximum acceptable value for this parameter was fixed at 4ns, FWHM.

3) Pre and late pulsing

Pre and late pulsing describes the deviation of the transit time distribution from the ideal gaussian shape. A limit on this deviation must be posed because of its possible dangerous effect on the e- vs. $\alpha$ identification, which is based on the scintillator pulse shape. Indeed, the presence of pronounced non gaussian tails in the transit time distribution can originate delayed anode pulses, that could be misinterpreted as delayed photons produced by the long response proper of an alpha particle.

4) Afterpulses

As pre and late pulsing, afterpulses can pose a serious problem because they obviously mimick the delayed signals expected from alpha particles. The probability of afterpulsing is particularly important in the region from 50 ns up to about 1 $\mu$s, that is the region potentially viable for the pulse shape discrimination.

5) Dark count rate

This parameter has a twofold impact on the experimental features of Borexino. On one hand it determines the minimum number of coincident tubes, included in the trigger definition to reduce the random trigger rate within very low limits; on the other hand it is a further factor potentially

masking the alpha identification. In fact a too high rate would produce random pulses that could mix the different timing patterns of electrons and alpha particles.

6) Single photoelectron pulse height resolution

A clearly visible peak in the single electron response would be of great help. It can assure an accurate threshold setting for each channel and a careful stability monitoring of the tubes performances during the operation.

The original specification for this parameter was a peak to valley ratio of at least 1.1. This is the minimum value allowing for a still (hardly) visible peak.

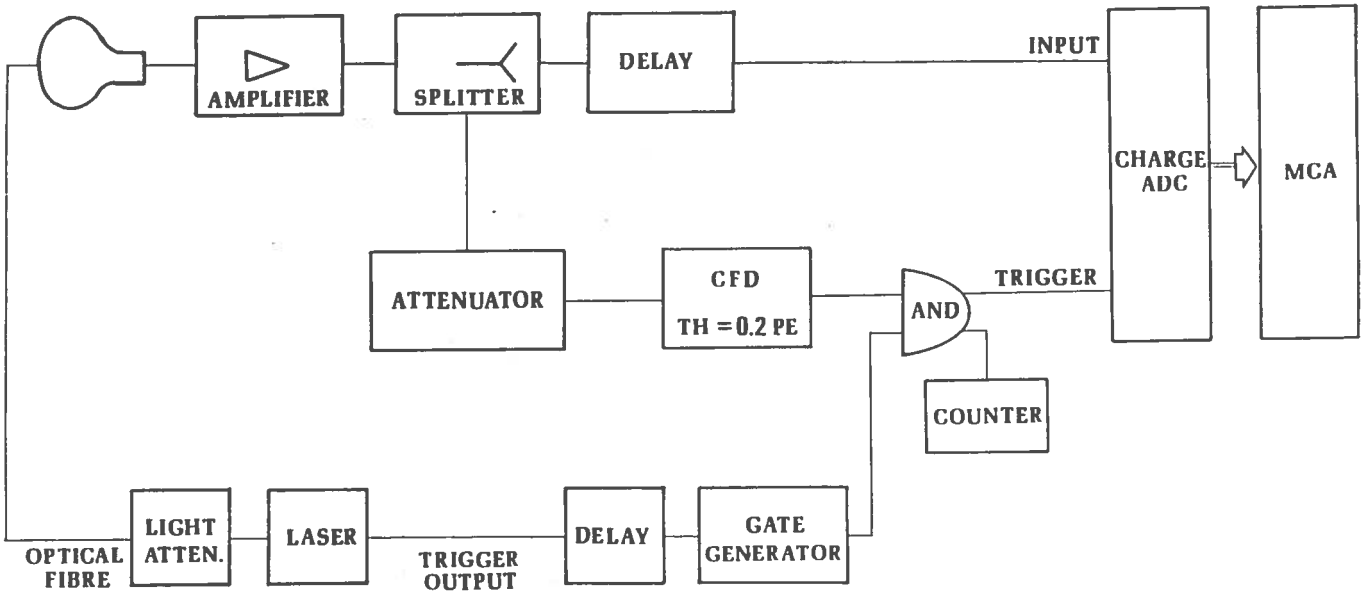


*Figure 1. Block diagram of the experimental set-up used for the single electron response measurement.*

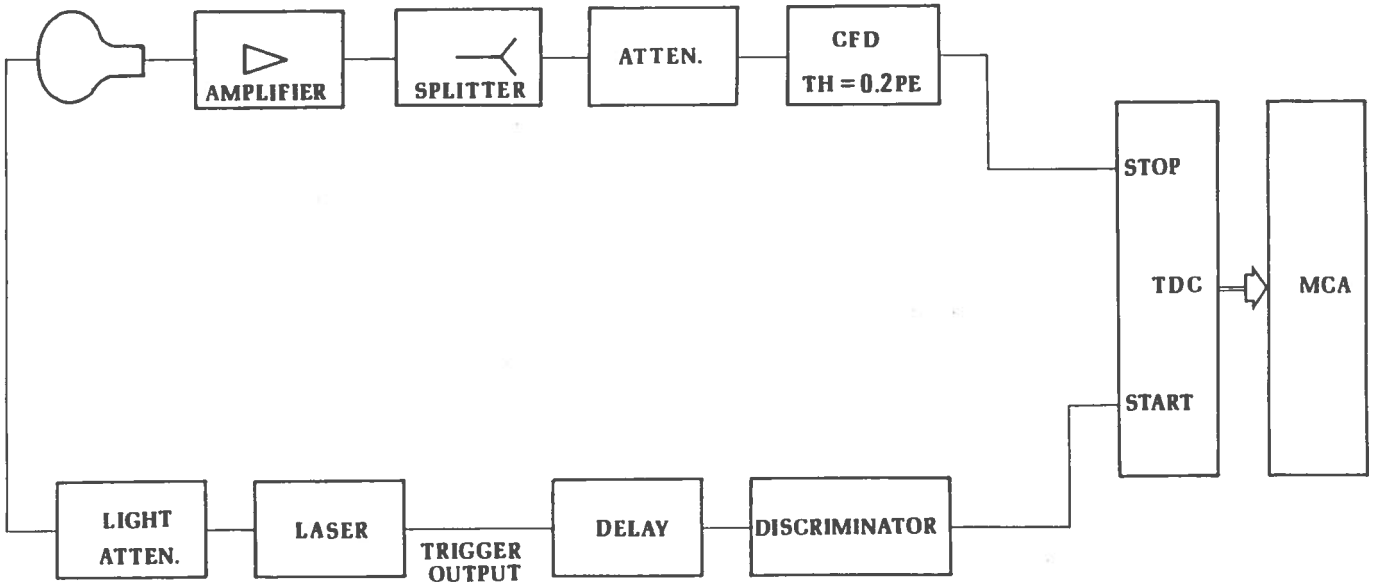


*Figure 2. Block diagram of the experimental set-up used for the transit time distribution measurement.*

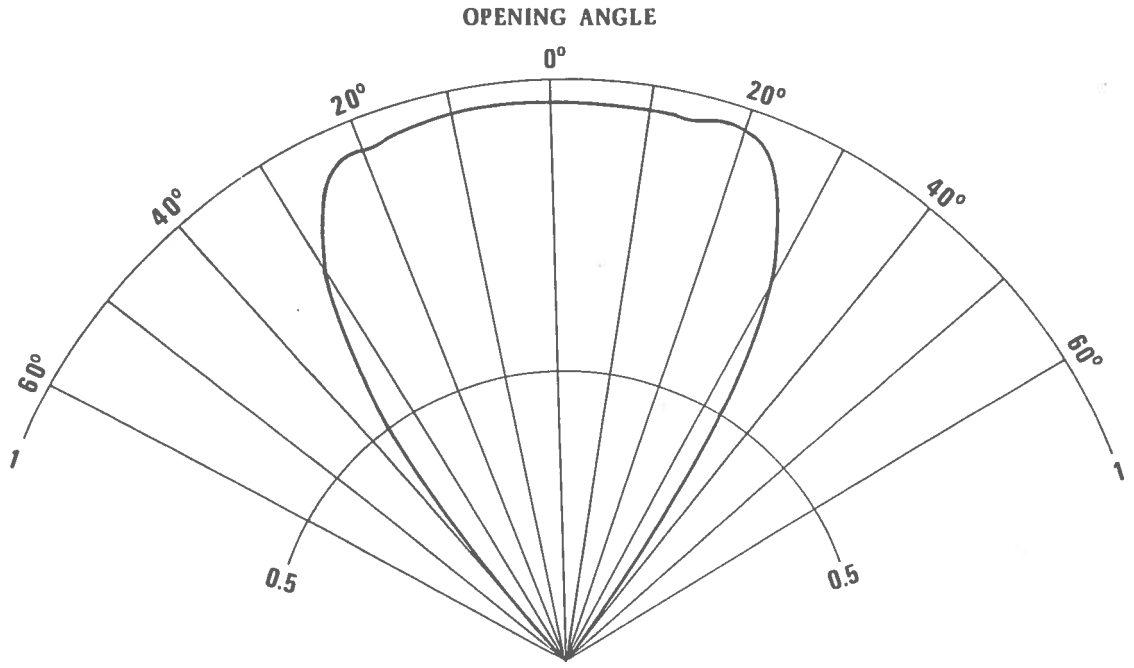


*Figure 3. Light emergence pattern of the fibre end*

The comparative analysis of the four available tubes, on the basis of the above listed parameters and the related considerations, has been performed both through the direct measurements of some samples of the candidate photomultipliers, carried out by members of the collaboration, and through the comparison of the minimum guaranteed values as specified by the manufacturers.

## 3. - EXPERIMENTAL SET-UP

The quantum efficiency of the tubes has not been measured, and only the values provided by the manufacturers have been taken into account.

The other parameters but the afterpulses have been measured with an experimental set-up based on a Hamamatsu PLP-01 picosecond light pulser, emitting blue light at a wavelength of 410 nm.

The schematic block diagrams of the measurement set-ups for the single electron response and the transit time spread are reported in figures 1 and 2.

The light is guided to the photomultiplier, operated in a black box, from the output window of the diode head of the laser through a fibre optic light guide, whose end is 1.5 m far from the cathode surface. This distance is enough to produce a uniform full photocathode surface illumination, since the light emerging from the fibre follows an irradiance profile having a semi-aperture angle of more than 20 degree (see figure 3).

Furthermore, the light is properly attenuated to be sure that only single photons hit the photocathode. Indeed, in Borexino the tubes detect only single photons in most of the cases.

In order to attenuate the light a very simple system has been devised, which exploits the diverging aperture of the light from the fibre. The end of the fibre coupled with the laser head goes inside a black hollow cilinder whose internal diameter is equal to that of the fibre. Another fibre, inserted on the other side of the cilinder, collects the light from the first and conveys it to the photomultiplier. Both the fibres can slide in the hollow cilinder, so that their distance can be conveniently adjusted. Taking into account the characteristic irradiation pattern of figure 3, the second fibre collects only a fraction of the light escaping from the first; the amount of this portion depends upon their distance, thus resulting in a controlled attenuation of the intensity of the light impinging upon the photocathode.

The anode signal is linearly amplified and then splitted through a 50 ohm matched splitter. In the scheme in figure 1, (single electron response measurement), one of the splitter outputs, properly delayed, feeds the signal input of a charge ADC, while the other is used to derive the trigger signal which opens the integration gate of the ADC itself. Actually, the trigger for the ADC comes from an AND unit that seeks for a coincidence between the constant fraction discriminator output and the signal coming from a gate generator, activated by the laser. In such a way only anode pulses sinchronized with the laser are allowed to produce the trigger for the ADC, and hence the histogram displayed on the multichannel analyzer connected to the ADC is the true light induced single electron response, virtually not contaminated by unwanted dark noise pulses.

It is possible to adjust the threshold of the constant fraction at the level to be used later for the transit time spread measurement. Indeed, if we increase the constant fraction threshold, initially set at its minimum level, the lower part of the spectrum is cut. The threshold is then adjusted so that the starting edge of the residual portion of the spectrum is located in a channel which be 0.2 times the channel of the peak of the distribution (0.2 pe).

The counter shown in the figure 1 is used to measure the relative count rate variation described later in the frame of the magnetic field sensitivity tests; it can be used also to measure the dark count rate above the 0.2 pe threshold, by disabling the input of the coincidence unit coming from the laser trigger.

The transit time measurement set-up (figure 2) is very straightforward: the start signal for the TDC is directly derived from the trigger output of the laser and the stop comes from the output of the constant fraction discriminator with the threshold adjusted at the level of 0.2 pe (obviously the unused output of the splitter in the figure is terminated by a 50 ohm matched terminator).

It must be pointed out that the intrinsic low jitter (10 ps) between the laser light pulse and the trigger signal, combined with the extremely narrow width of the light pulse (fwhm<50ps), allows to perform very accurate measurements of the transit time spread of the tubes.

In order to compare the measurements performed on the different tubes, the applied high voltage has been individually adjusted so to achieve a multiplier gain of ~ $10^7$, which corresponds to the gain that will be adopted in the actual experimental situation.

## 4. - LIGHT LEVEL ADJUSTMENT FOR THE SINGLE PHOTON ILLUMINATION MEASUREMENT

The single photon illumination condition is obtained in two different ways.

In the first procedure the dark noise spectrum is assumed as reference. This spectrum is made of pulses originated by thermoionic electrons escaping both from the dynodes and from the photocathode. The latter, in particular, produce a peak in the histogram of the anode pulse charge which is approximately in the same position as that originated by single photon excited pulses. Thus, this peak can be assumed as a sort of autocalibration tool provided by the tube itself.

In fact, by comparing this spectrum to that recorded when the tube is illuminated by the the laser, it is possible to decide when the light is attenuated enough to reach the single photon illumination condition; this is achieved when the light excited spectrum has a peak almost in the same position as the dark spectrum.

The two peaks, in the dark spectrum and in the light excited one, can be slightly displaced each other, as a consequence of the non negligible occurrence of a thermoionic emission from the dynodes affecting the former. This emission adds a contribution concentrated in the first channels, having the twofold effect of partially masking the peak and of changing its location.

On the other hand, in the light excited spectrum, the contribution of low level anode pulses, originated from photoelectrons erroneously impinging onto dynodes following the first or skipping some amplification stages, is much smaller: its impact on the peak position is less important. This is the reason why the two peaks, even though close each other, can be however reciprocally displaced.

The second procedure adopted to confirm the achievement of a proper illumination condition requires a comparison between the number of the output pulses per second from the anode of the tube and the number of triggers per second from the laser.

As empirical rule, a good single illumination condition is achieved when the ratio of output pulses to trigger pulses is at least less than 5%.

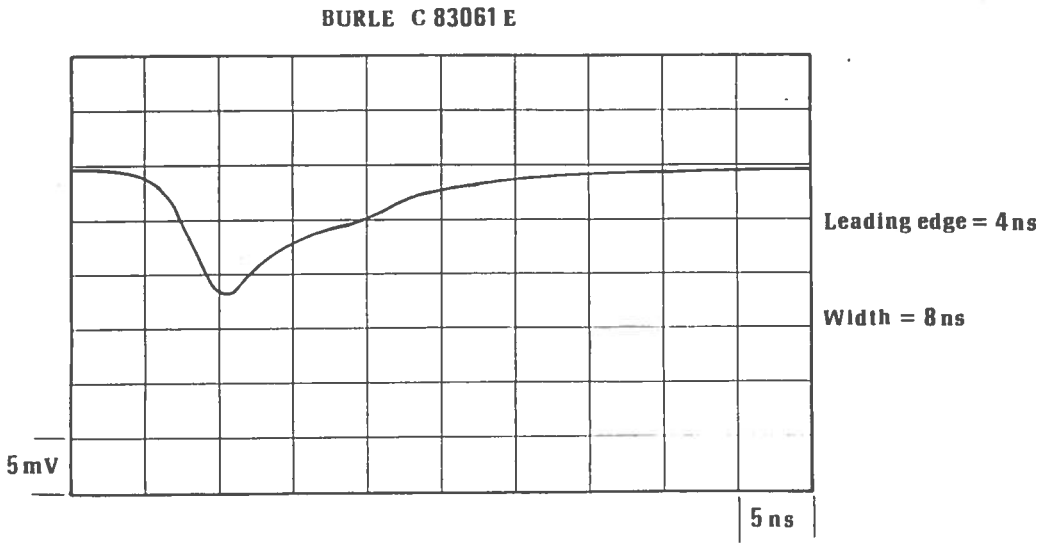


*Figure 4. Shape of the single electron anode pulse of the Burle C83061E*

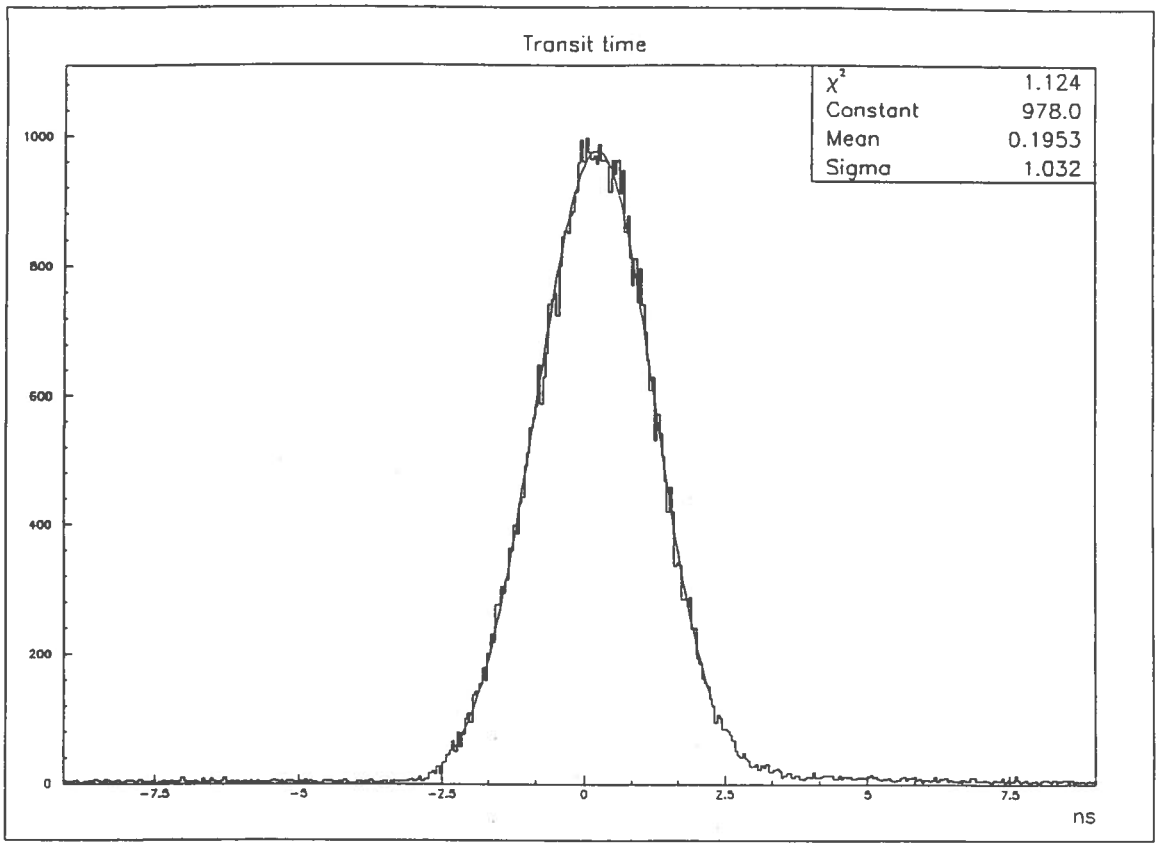


*Figure 5. Transit time distribution of the Burle C83061E*

## 5. - BURLE C83061E

### 5.1. - General features

The Burle C83061E is characterized by a photocathode having a radius of curvature of approximately 20.1 cm, a minimum useful photocathode diameter of 23.5 cm, and thus a minimum projected cathode area of 434 $cm^2$. The half angle subtended by the curved photocathode is about 21 degree. The weight of the whole tube is around 4.4 Kg, of which 2,7 Kg concerns the glass.

The photocathode material is of the conventional bialkali type (CsKSb), producing the highest possible output in the blue region of the visible spectrum. The linear focussed multiplier structure comprises 12 dynodes.

A unique feature of this tube is the high gain gallium phosphide first dynode, which allows a very good resolution for the single photoelectron response. The remaining dynodes in the chain are made with conventional Cu-Be material.

### 5.2. - Anode pulse shape

The shape of the anode pulse is shown in figure 4. The anode signal is narrow and fast, being characterized by a leading edge of 4 ns and by a width at fwhm of 8 ns.

### 5.3. - Transit time spread

The transit time distribution obtained measuring a sample of the tube is reported in figure 5. The best fitted gaussian to the histogram of the measured data shows a sigma of ~ 1ns, with an estimated uncertainty of ~ 0.05 ns.

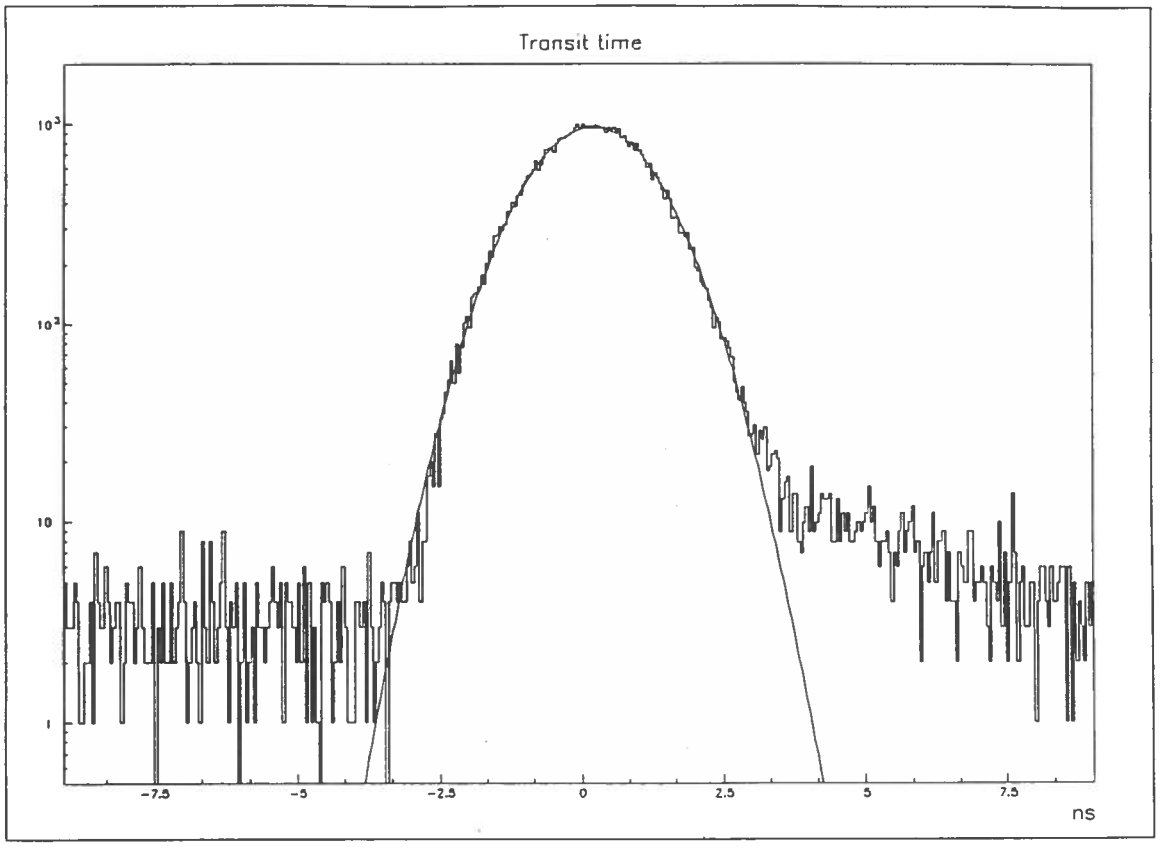


*Figure 6. Log plot of the transit time distribution of the Burle C83061E*

This result shows the intrinsic limited transit time spread of the tube.

5.4. - Pre and late pulsing

The curve in the figure 5 can be analyzed to derive the deviation shown by its tails from an ideal gaussian shape. It is worth to point out that the gaussian fit mentioned in the previous paragraph has been restricted only to the central portion of the curve, in order to achieve a satisfactory value of the $\chi^2$.

From the log plot of both the distribution and the fitted gaussian reported in the figure 6 it emerges that pre pulsing are not present, the flat component on the left side being a bakground contribution due to random noise coincidences, while there is evidence of late pulsing occurrence.

The late pulsing can be numerically expressed as the ratio between the total number of extra counts in the tail, (the difference between the counts in the tail of the experimental distribution and that in the best fitted gaussian) and the counts in a $\pm$ 3 $\sigma$ region of the fitted gaussian. To this purpose the span of the tail range is assumed equal to 20 $\sigma$; its starting point coincides with the instant where the experimental curve begins to deviate from the fitted gaussian: in this case 2.7 ns after the peak. Obviously this evaluation must be performed after the background estimation and subtraction.

The result of this analysis is a late pulsing content of about 3.5%.

5.5. - Afterpulses

Afterpulsing analysis has been focused to the three time intervals, after the main pulse, ranging from 4 ns to 30 ns, 30 ns to 100 ns and 4 ns to 900 ns.

This measurement, regarding afterpulses following single photoelectron main pulses, has been performed with the threshold for afterpulsing set to 0.1 pe. The pulses has been captured with a fast transient digitizer and written on tape. 30000 pulses has been registered and afterward software-analyzed. Dark noise induced random coincidence has been estimated and subtracted.

The results are reported in the table I.

*Table I - Measurements of the afterpulses for the Burle C83061E*

| Time interval | 4ns - 30 ns | 30 ns - 100 ns | 4 ns - 900 ns |
|---|---|---|---|
| Afterpulsing probability | 2.8 ± 0.2% | 1.7 ± 0.2% | 7.6 ± 0.4% |

These data indicate that the afterpulsing of the tube, even though limited, is however not totally negligible.

5.6. - Dark counts and spectrum

Dark noise count rate has been measured on two samples of the tube at ambient temperature (about 20°C), with a discriminator threshold set at 0.2 pe, and after a week of operation at least in complete darkness. The results are ~ 6000 Hz and ~ 4500 Hz, respectively.

Also the dark noise spectrum has been measured (figure 7).

Two key features of this histogram must be underlined: first, the narrow, single thermoionic electron peak exhibiting an extremely limited width and a very good peak to valley ratio; second, the not negligible count content in the region above the single photon, mainly due to the background contribution of U, Th and especially Potassium in the heavy glass envelope.

The excellent peak featured by this distribution is originated by the characteristics of the high gain gallium phosphide first dynode, an electron negative affinity material used to manufacture tubes with superior pulse height resolution.

5.7. - Single electron response

The exceptional peak featured by the tube in the dark noise spectrum is confirmed by the single electron response taken while exciting the photocathode with the laser light.

The measured spectrum is reported in figure 8. The peak to valley ratio and the width (espressed as the ratio of the sigma to the mean value) are 3.4 and 24.5% respectively.

These numbers demonstrate quantitavely the very good performances of this tube in term of single photoelectron pulse height resolution.

5.8. - Magnetic field sensitivity

All the measurements shown up to now have been performed in zero magnetic field conditions, obtained after compensation of the Earth's field. However some of the performances of the

photomultiplier have been measured also applying static magnetic fields of known intensities and directions, through the use of a double set of vertical and horizontal Helmholtz coils.

The parameters which have been measured to probe the tube sensitivity to the magnetic field are: the degradation of the single photoelectron pulse height resolution; the broadening of the transit time distribution under the effect of increasing values of the external field from 0 to 500 mG; the relative decrease of the effective detection efficiency of the tube, for a given detection threshold. This last measurement has been done: first recording the anode pulse counting rate, with the constant fraction discriminator threshold set at the usual level of 0.2 pe and with zero magnetic field; and then observing the decrease in the count rate following the increasing of an applied field.

In figures 9 and 10 the single photoelectron transit time distributions for an applied field of 500 mG, parallel respectively to the x and y axis, are reported. The axis are defined as in the figure 11. No measurements have been taken for fields parallel to the z axis, that however is the direction less sensitive to the magnetic field.

From the figure 9 it can be desumed that the field parallel to the x axis does not affect the width of the distribution, but causes an enhancement of the tail on the right side of the curve. On the other hand the figure 10 shows that the field of 500 mG, when parallel to the y direction, completely destroys the timing of the tube, causing the growth of several peaks in the transit time distribution.

These results confirm the well known property of the photomultipliers equipped with linear focussed dynode structures that the field parallel to the y axis is the one most affecting the tube performances.

This intrinsic behaviour of the tube is confirmed by the measurements of the single photoelectron reponse.

The relevant results for an applied field of 500 mG parallel to the x and y axis are reported in figures 12 and 13. While in the former a peak is still present, even though extremely degraded with respect to the results with no magnetic field, in the latter the peaked structure is completely lost. Finally, in figure 14 the count rate variation for applied fields parallel to the three axis of intensities from 0 to 500 mG is reported.

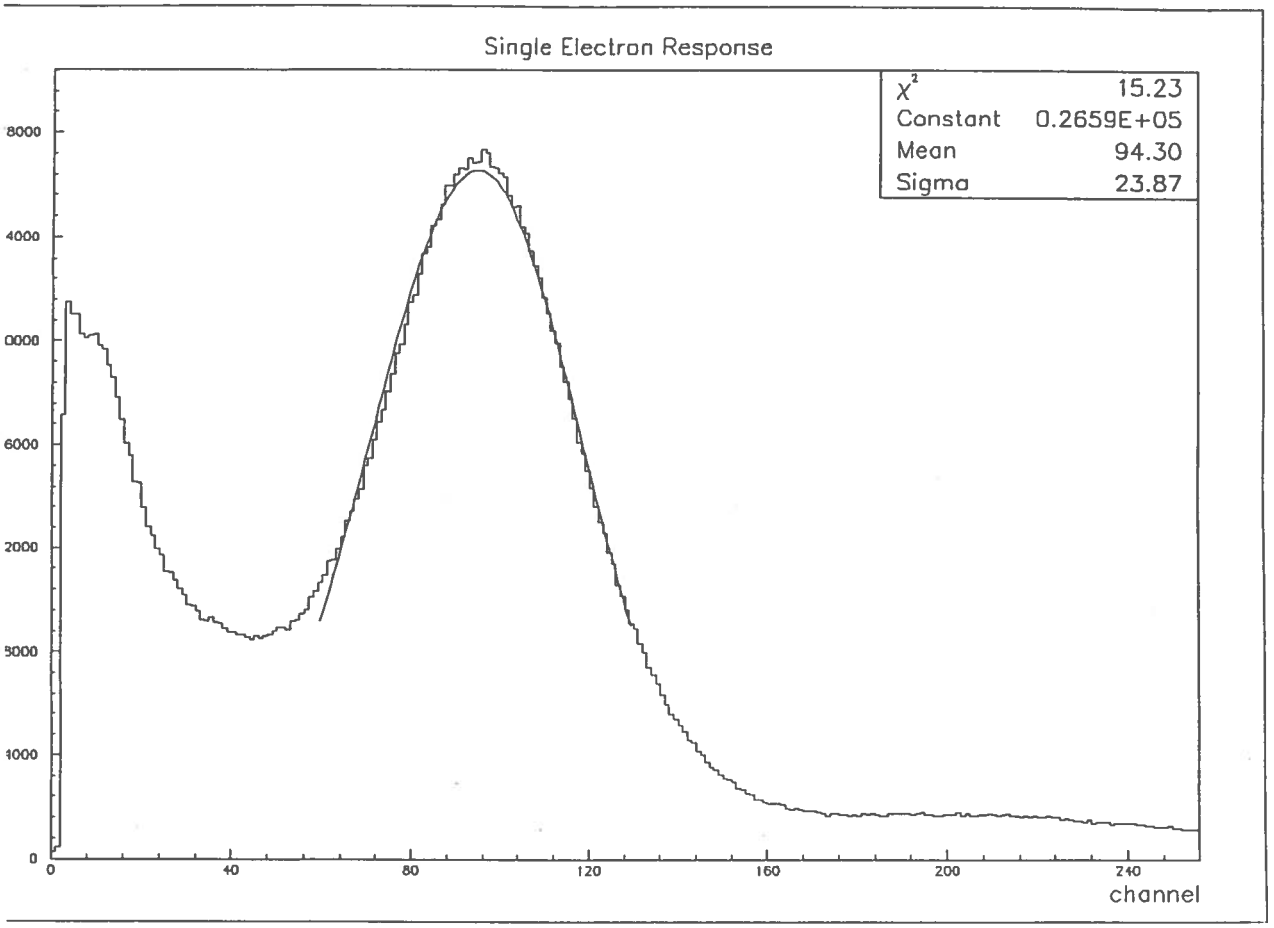


*Figure 7. Dark noise spectrum of the Burle C83061E*

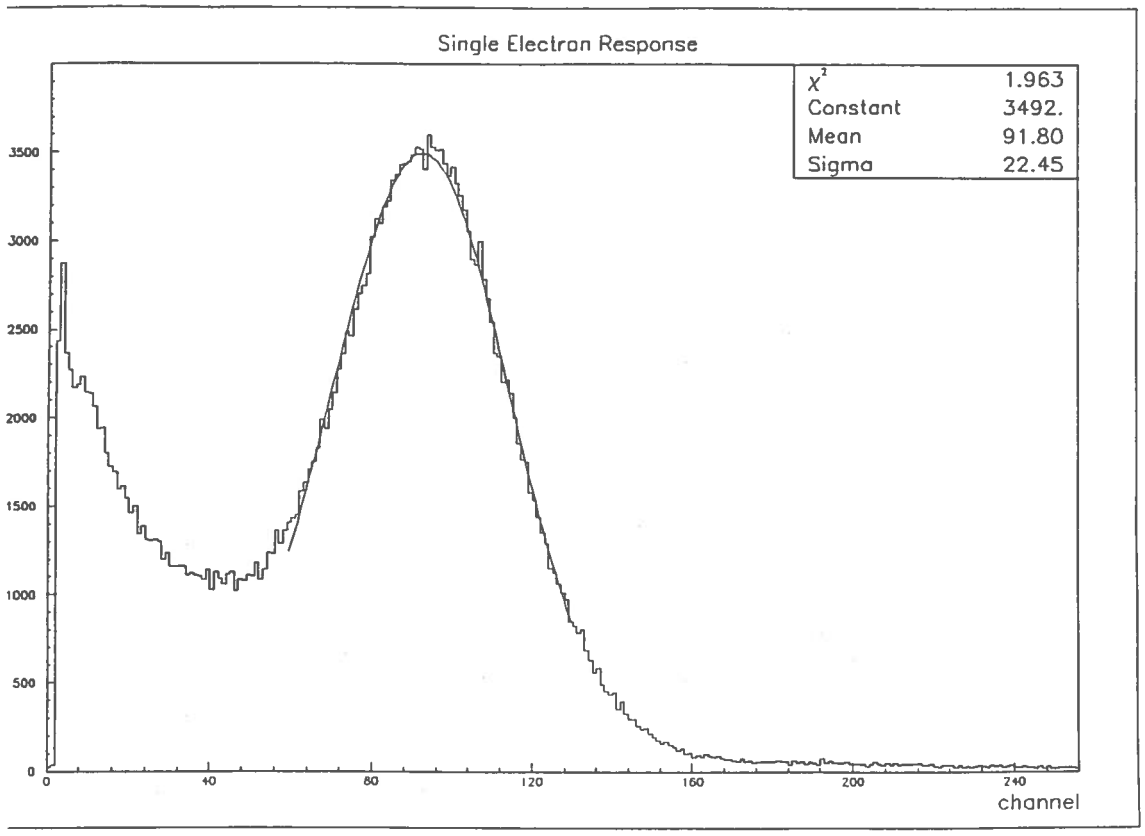


*Figure 8. Single electron response of the Burle C83061E*

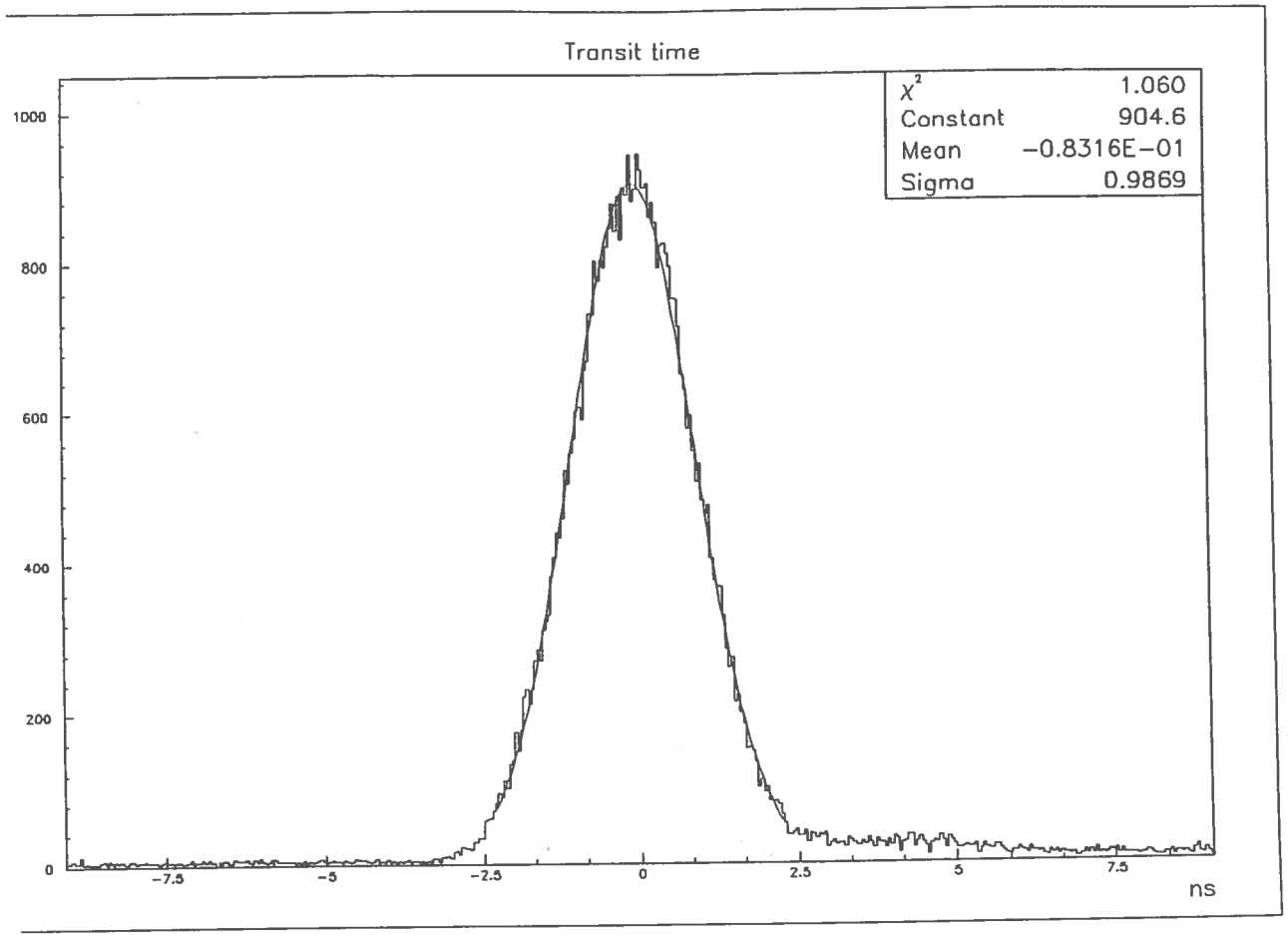


*Figure 9. Transit time distribution of the Burle C83061E for an applied magnetic field of 500 mG parallel to the x axis.*

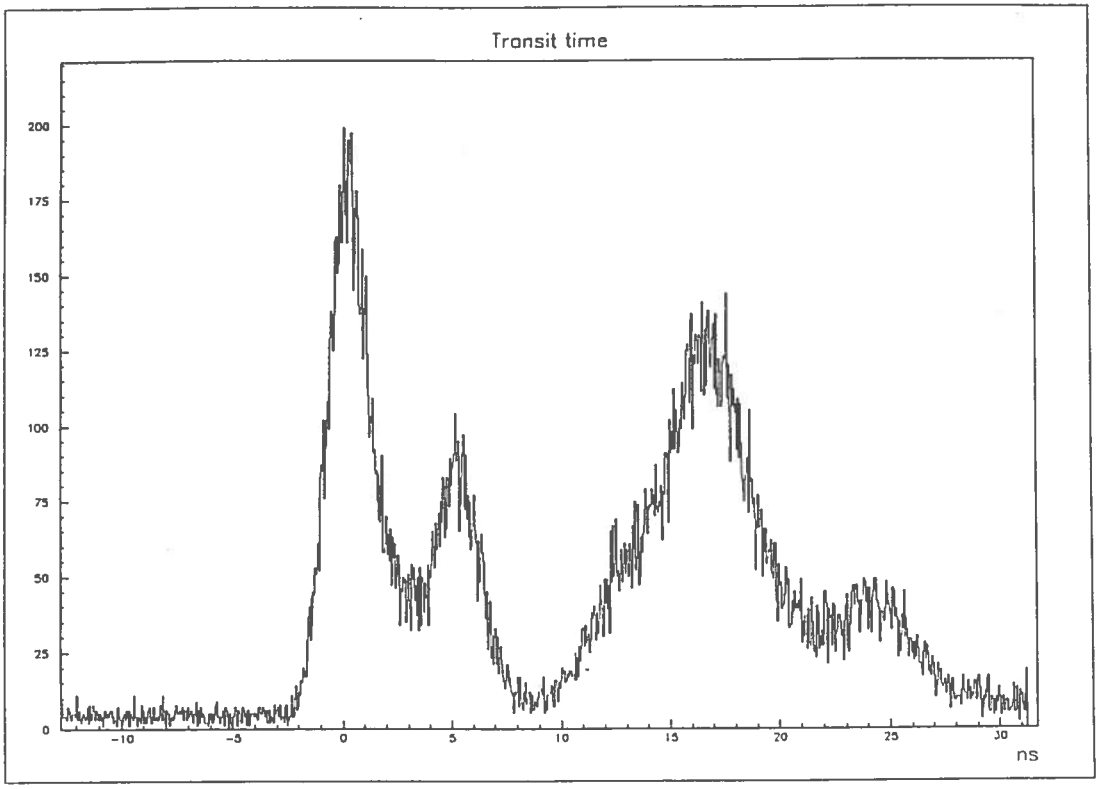


*Figure 10. Transit time distribution of the Burle C83061E for an applied magnetic field of 500 mG parallel to the y axis.*

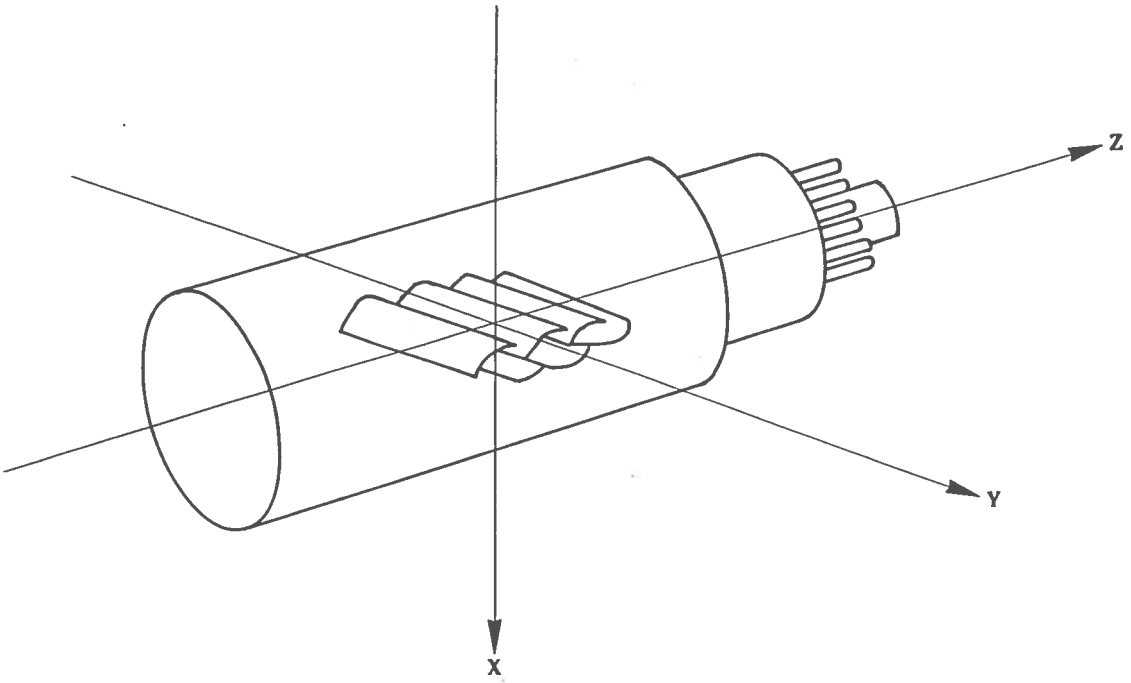


*Figure 11. Definition of the x, y and z axis for a phototube with linear focussed dynode chain.*

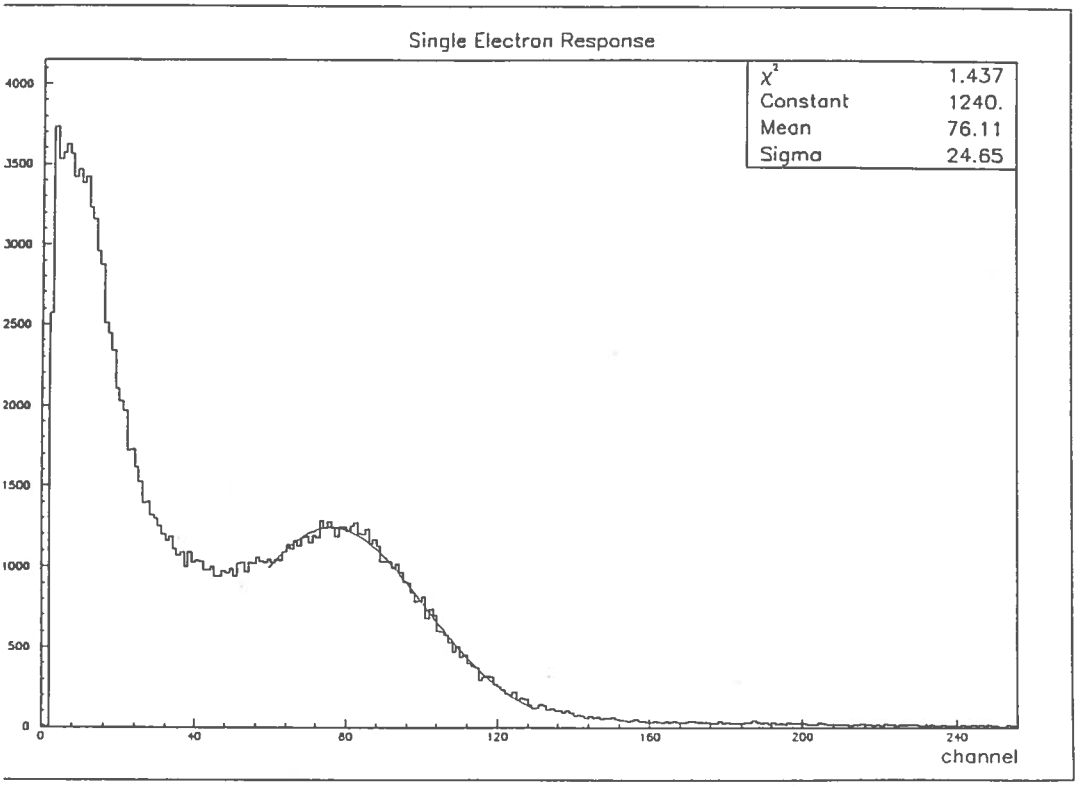


*Figure 12. Single electron response of the Burle C83061E for an applied magnetic field of 500 mG parallel to the x axis.*


16

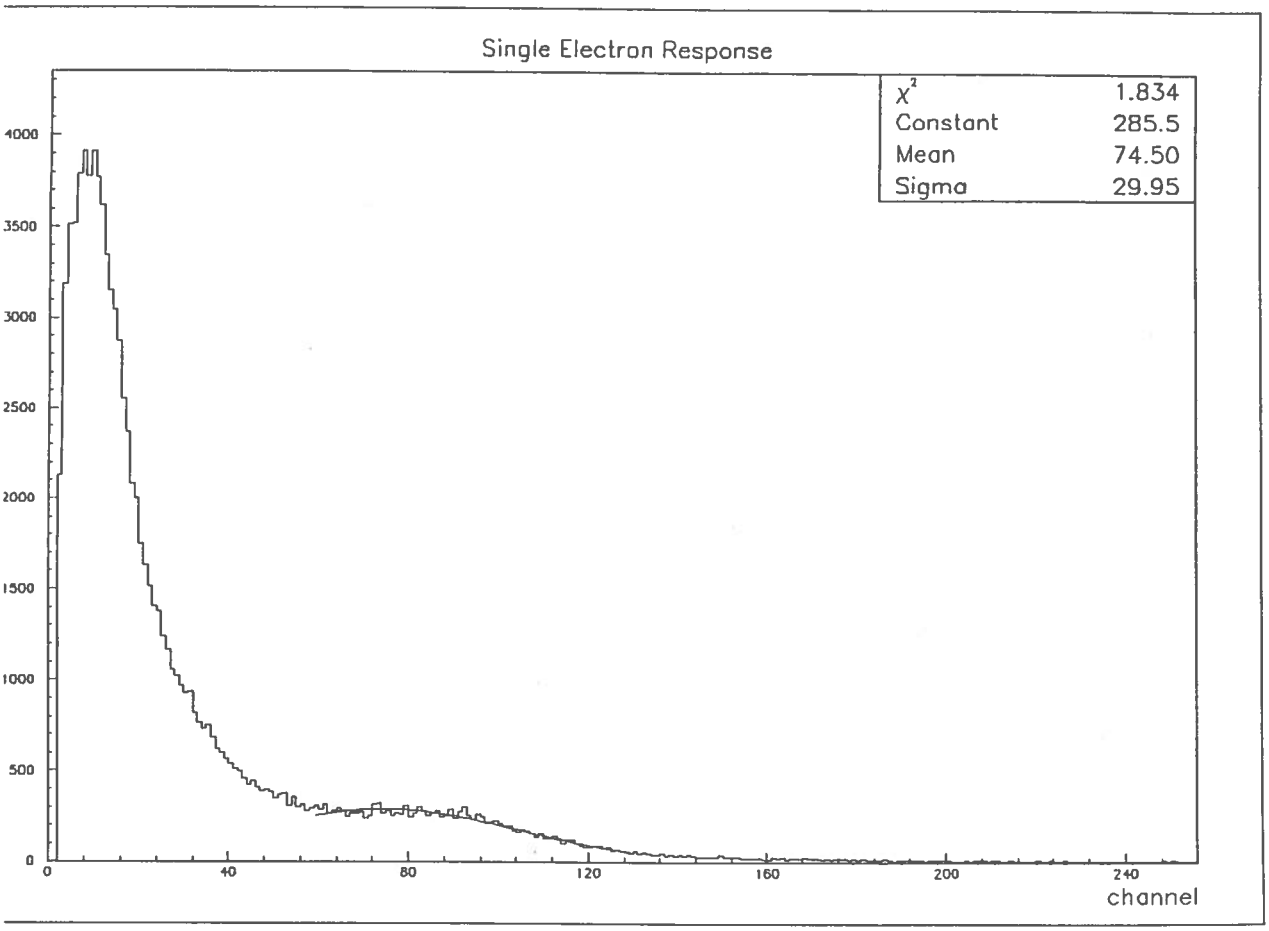


*Figure 13. Single electron response of the Burle C83061E for an applied magnetic field of 500 mG parallel to the y axis.*

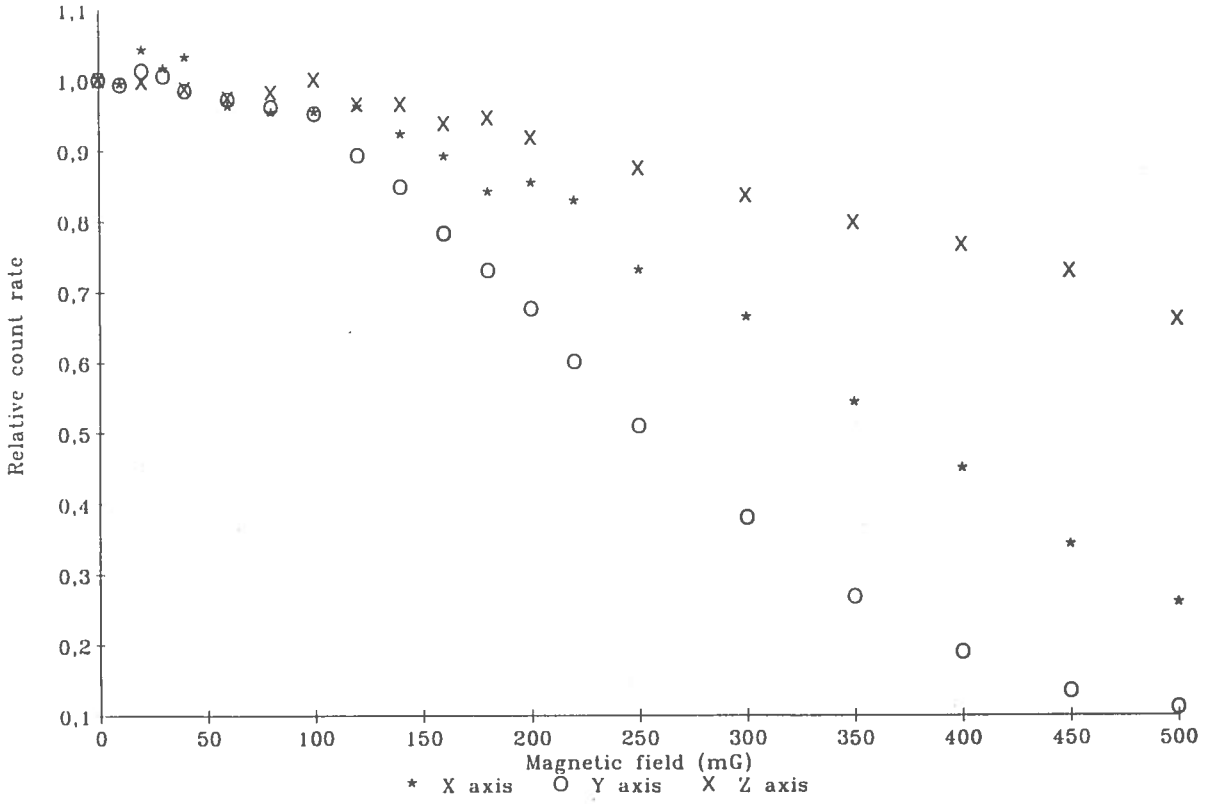


*Figure 14. Relative count rate variation for the Burle C83061E as function of the applied magnetic field.*

## 6. - HAMAMATSU R4558

### 6.1. - General features

The radius of curvature, the minimum useful diameter and the minimum projected area of the photocathode of the R4558 phototube are respectively 126 cm, 190 cm and 283 $cm^2$. The half angle subtended by the hemispherical photocathode is about 48 degree. The weight of the whole tube is around 900 g, of which 780 g is glass.

The Hamamatsu tube is realized with a conventional bialkali type (CsKSb) emissive cathode surface, which has been used also for the dynodes. It must be remarked that, contrary to the other candidate tubes, this one is characterized by a venetian blind dynode structure, consisting of 9 dynodes.

### 6.2. - Anode pulse shape

The shape of the anode pulse is shown in figure 15. The leading edge, 4 ns, and the width, 9.5 ns as FWHM, show the fast responding characteristic of the tube.

### 6.3. - Transit time spread

The results of the measurement of this parameter performed are shown in figure 16. The width of this curve is ~ 1.4 ns, as s of the best fitted gaussian overlapped to the experimental histogram. The uncertainty in the width estimation is about 0.05 ns.

This measure demonstrates the satisfactorily narrow dispersion of the transit time curve of this photomultiplier.

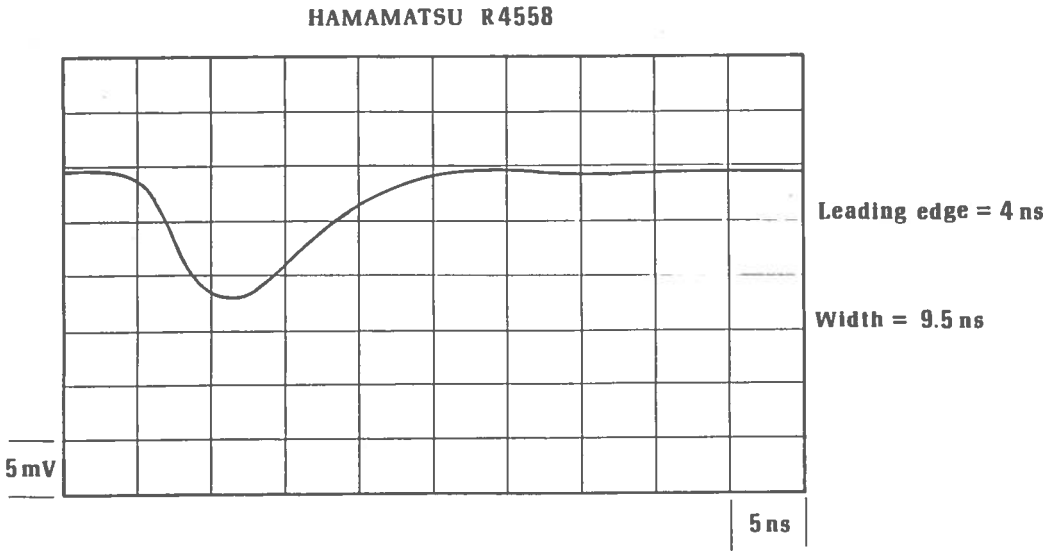


*Figure 15. Shape of the single electron anode pulse of the Hamamatsu R4558.*

6.4. - Pre and late pulsing

The figure 16 shows that the overall shape of the curve deviates from an ideal gaussian profile, as it is confirmed also by the $\chi^2$ value. The log plot of the distribution, reported in the figure 17, indicates no pre pulsing, while there is a tail on the right side of the curve.

The late pulsing, numerically quantified as explained in paragraph 5.4, is about 5%.

6.5. - Dark counts and spectrum

The dark count rate of the tube has been measured, after a suitable period of darkening, in the usual condition, i.e. ambient temperature of about 20°C and with the threshold set at the standard 0.2 pe level. The result obtained is a count rate of about 1100 Hz.

A typical dark noise spectrum is reported in figure 18. It must be noted the absence of a clear evident peak in this distribution.

6.6. - Single electron response

The profile of the spectrum of the single electron response is very similar to the noise spectrum (see figure 19). However, in this light induced distribution a peak is still visible, originating a peak to valley ratio of 1.1.

It must be pointed out that the presence in the single electron response of a not very evident peak is due to the adopted dynode structure. Indeed, the partitioned venetian blind dynode structure features a poorer pulse height resolution with respect to that of the linear focussed one.

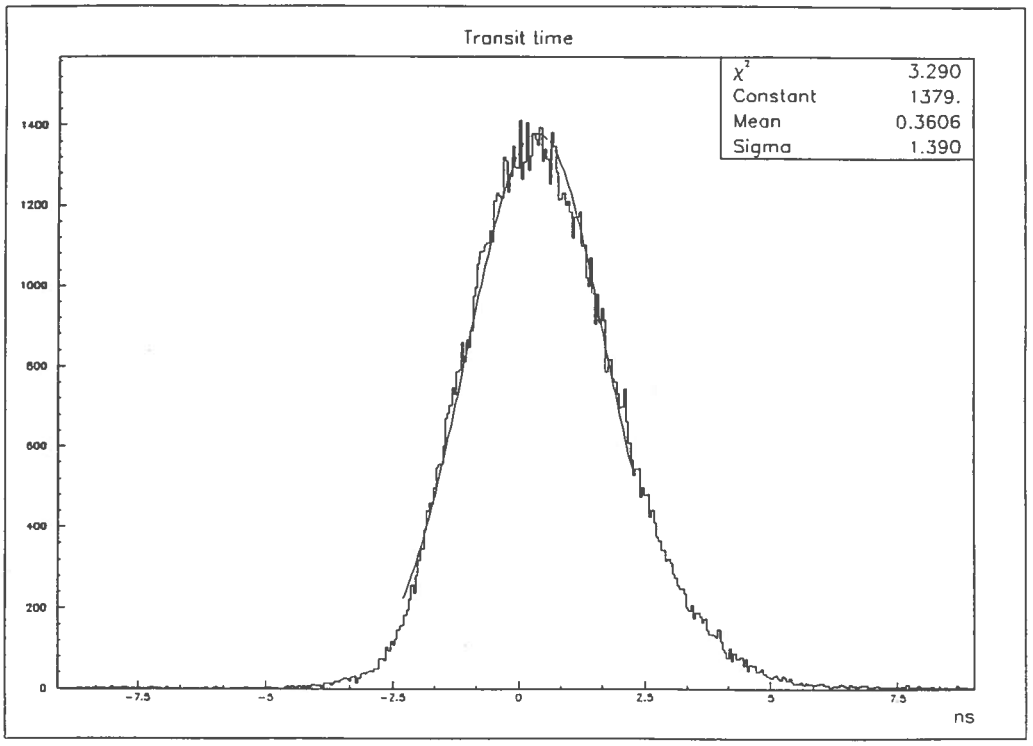


*Figure 16. Transit time distribution of the Hamamatsu R4558.*

6.7. - Magnetic field sensitivity

From figure 20 to figure 22 the single photoelectron transit time distributions for applied fields of 500 mG parallel to the three main axis of the tube are reported.

The axis definitiom is obviously different from that normally used for the linear focussed tubes. While the z axis is still the simmetrical axis of the tube, the x and y are respectively parallel and perpendicular to the venetian blind elements, as indicated in figure 23.

These results point out that the tube shows a very low sensitivity to the magnetic field. More in detail, it is interesting to note that, while the field parallel to the z axis practically do not affect at all the distribution, the field parallel to the x axis introduces a negligible worsening of the width of the distribution, and that parallel to the y axis produces a global distortion of its shape.

The single photoelectron responses, for the same applied fields in x and y directions, are reported in figures from 24 and 25 (the field parallel to the z direction does not influences the tube and the realtive measurements are strongly similar to that for the x direction). These measurements confirm on one hand the limited sensitivity of the tube to the magnetic field, and on the other that the y direction is the one most affecting the tube.

Figure 26 shows the relative count rate variation for magnetic fields parallel to the y and z axis, with values ranging from 0 to 500 mG. For the latter no drop of the count rate is observed, while for the former a 10% decrease is evident. The result of the measurement for the direction parallel to the x axis, not reported in the figure, closely resemble that desumed for the z one, with no detectable variation.

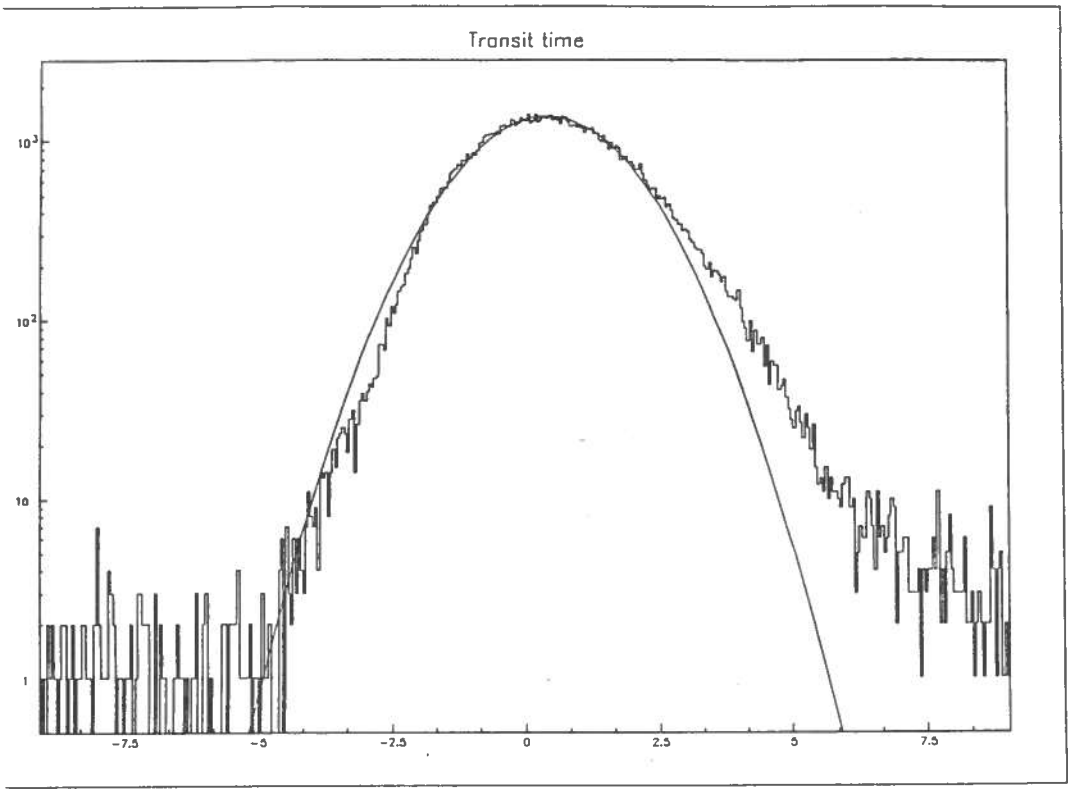


*Figure 17. Log plot of the transit time distribution of the Hamamatsu R4558.*

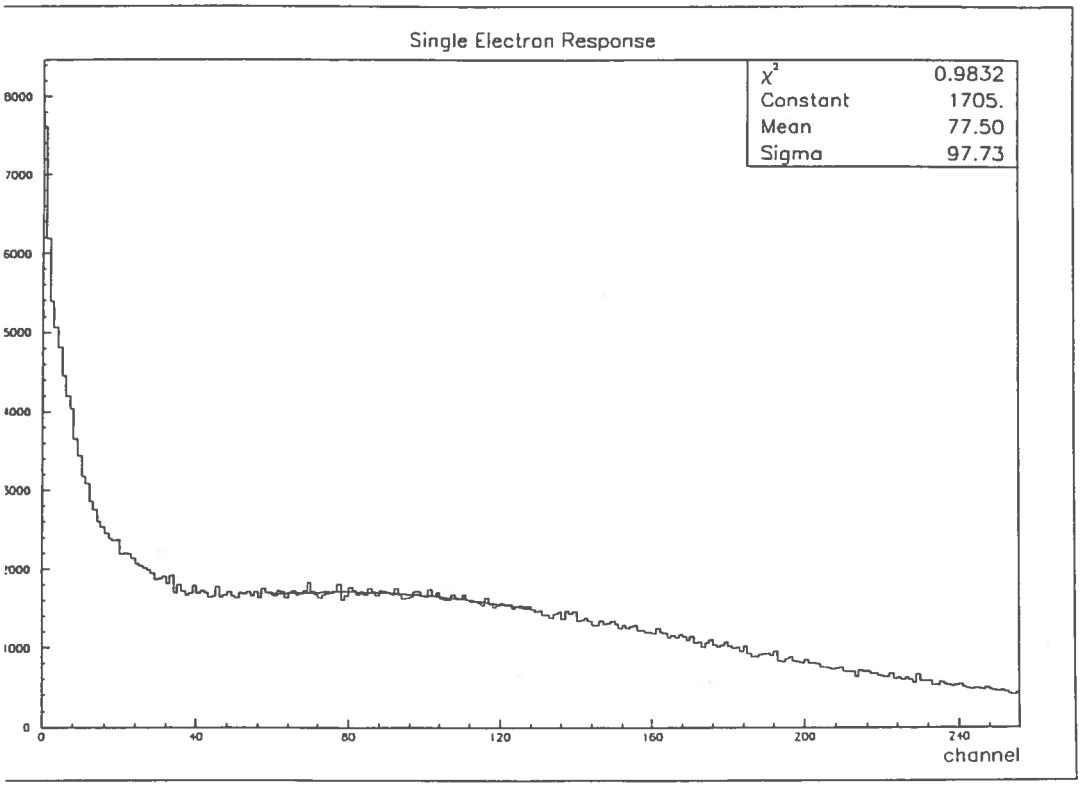


*Figure 18. Dark noise spectrum of the Hamamatsu R4558.*

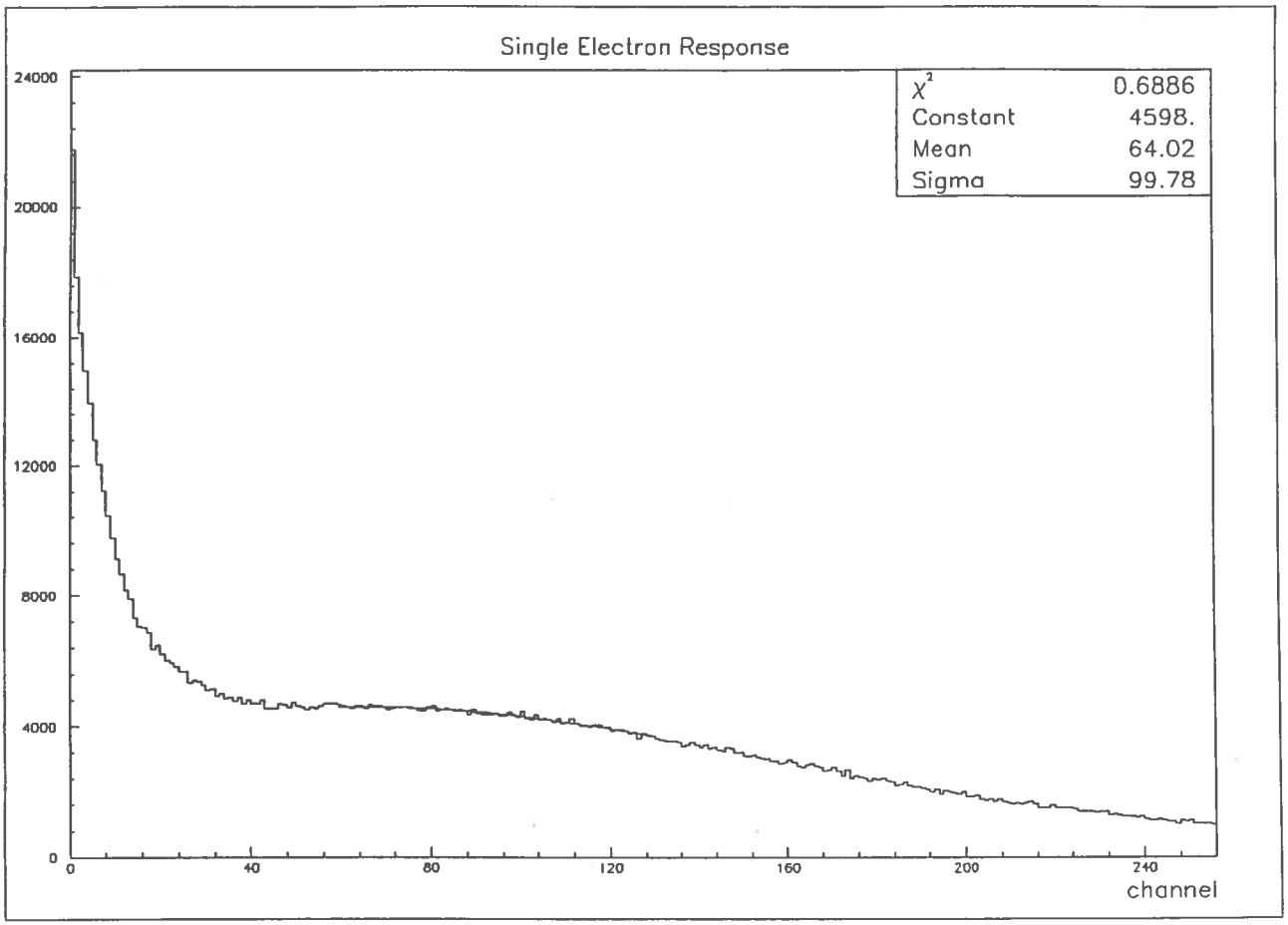


*Figure 19. Single electron response of the Hamamatsu R4558.*

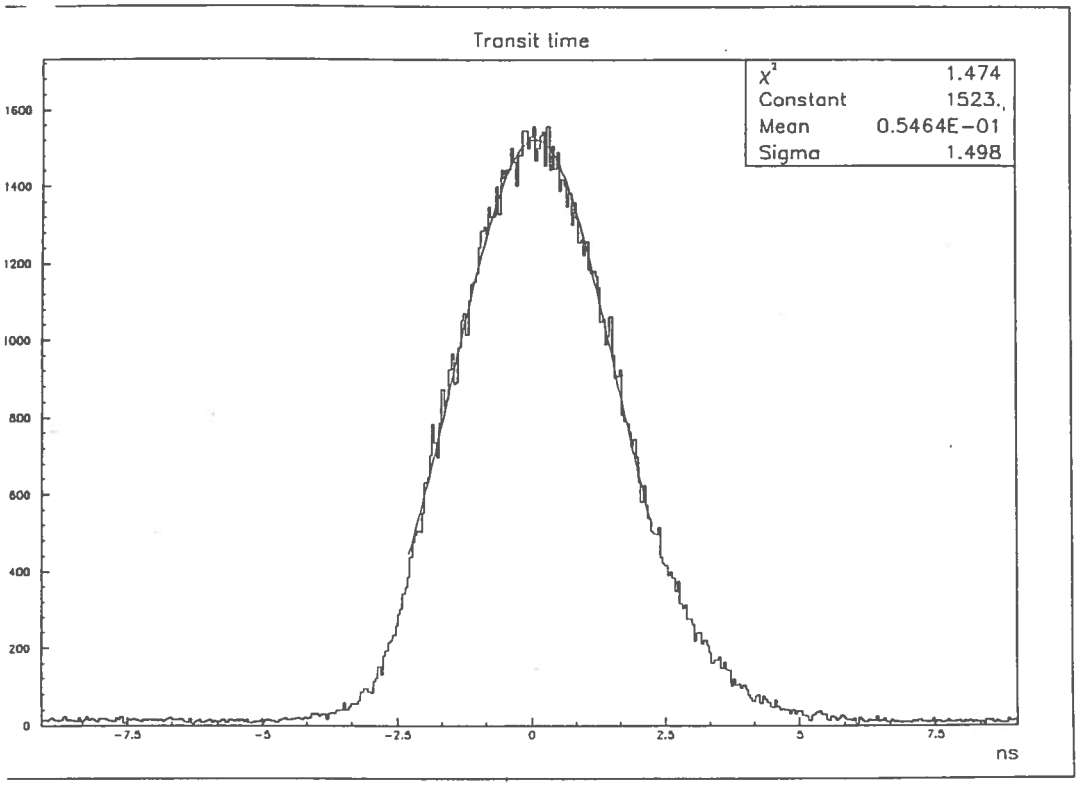


*Figure 20. Transit time distribution of the Hamamatsu R4558 for an applied field of 500 mG parallel to the x axis.*

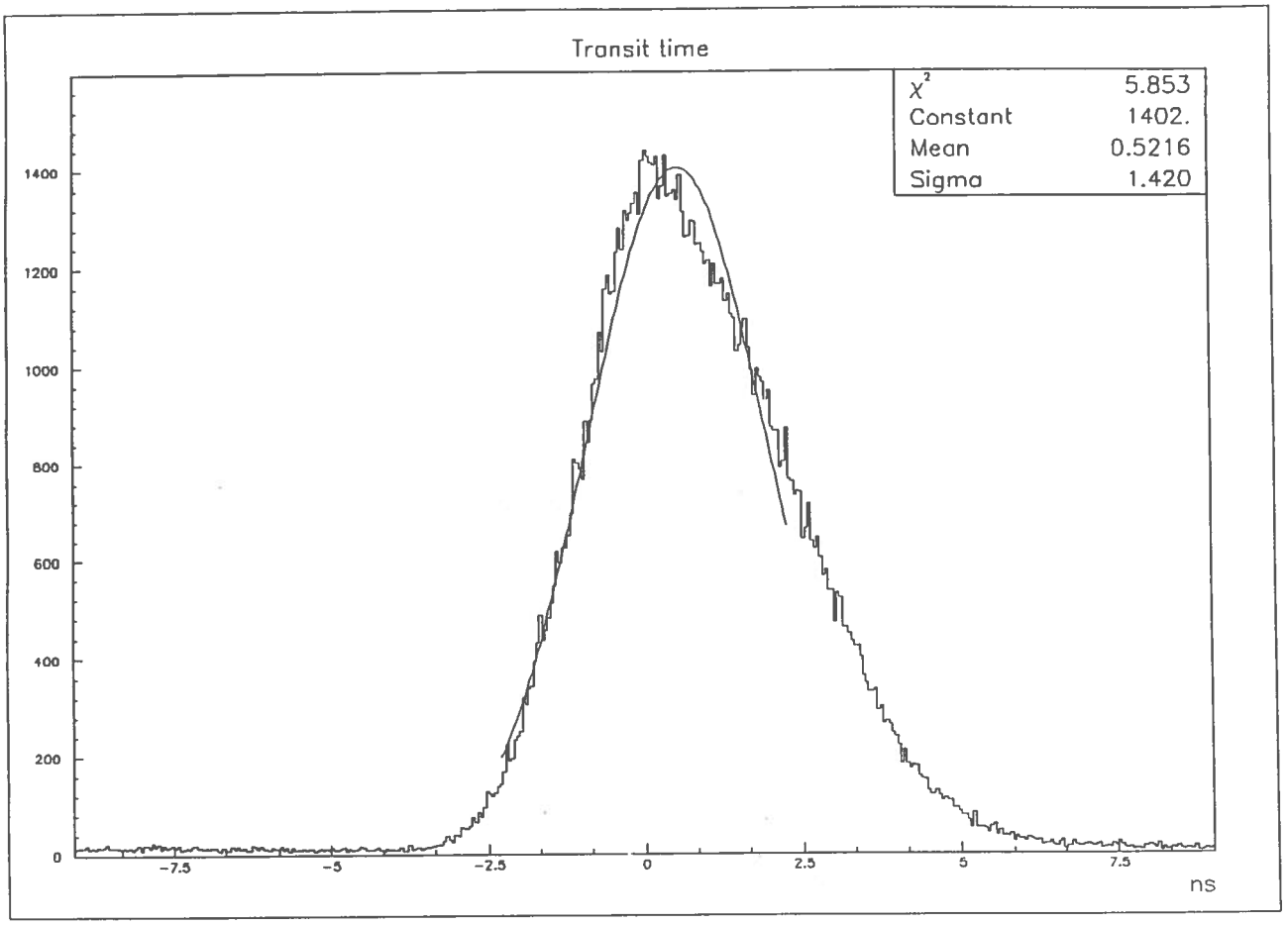


*Figure 21. Transit time distribution of the Hamamatsu R4558 for an applied field of 500 mG parallel to the y axis.*

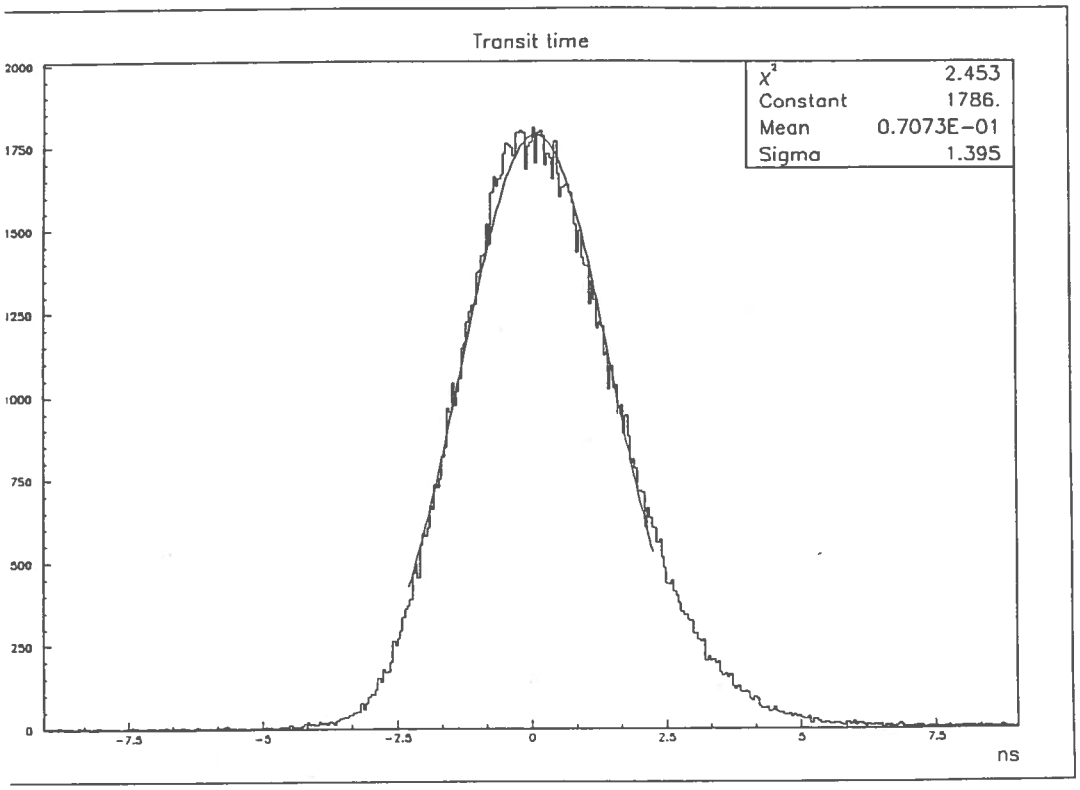


*Figure 22. Transit time distribution of the Hamamatsu R4558 for an applied field of 500 mG parallel to the y axis.*

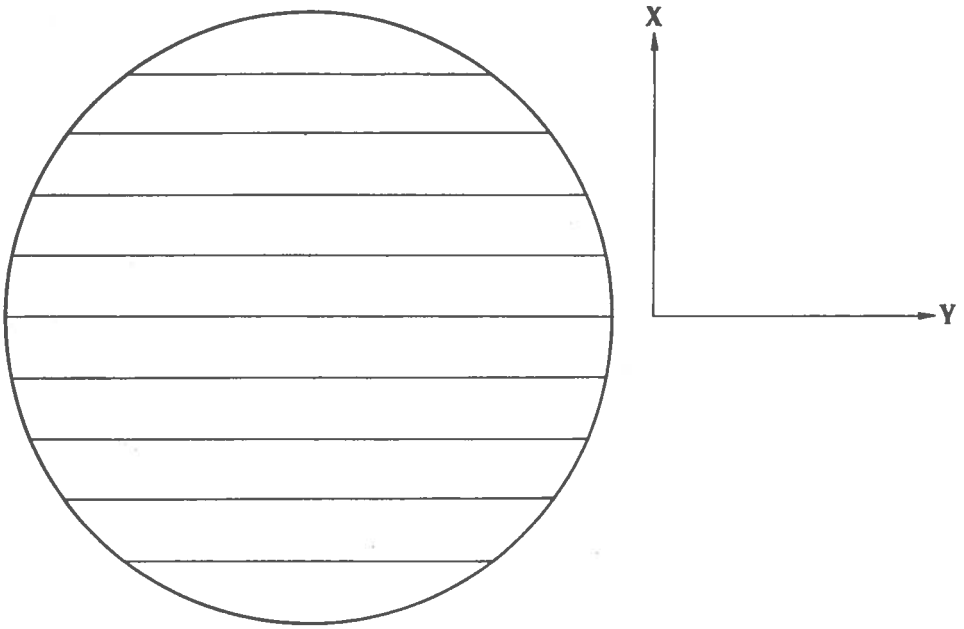


*Figure 23. Definition of the x and y axis in a venetian blind dynode structure.*

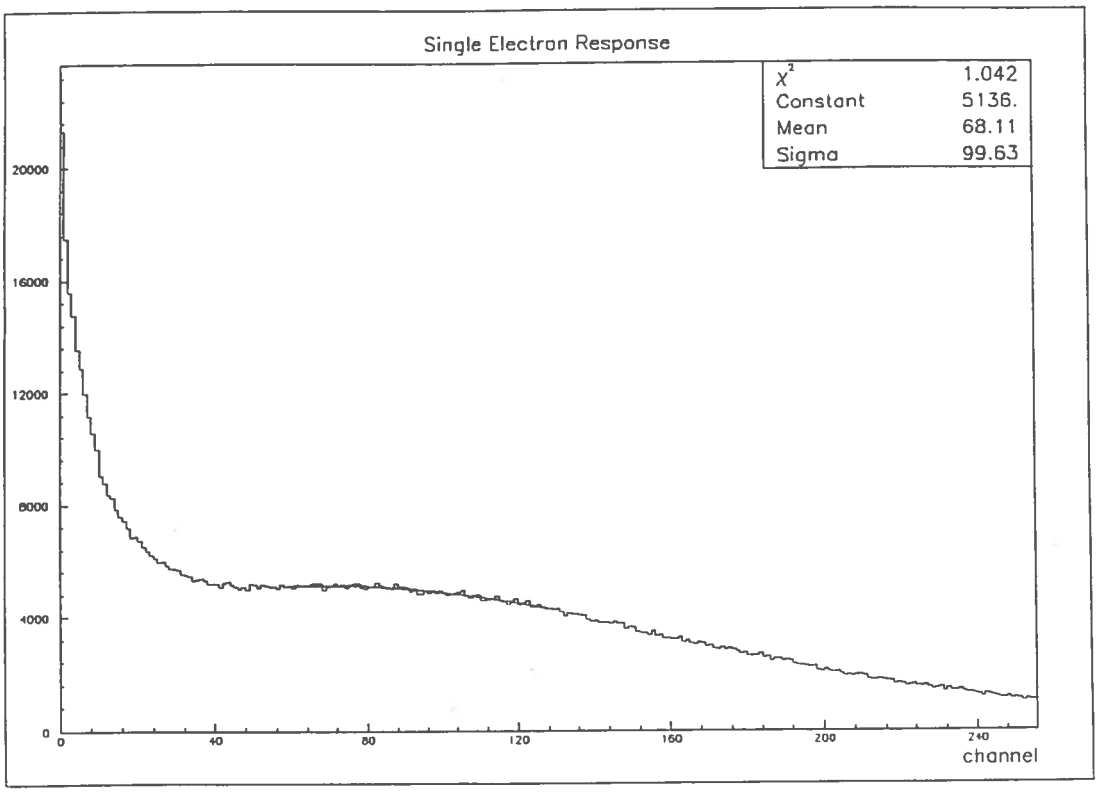


*Figure 24. Single electron response of the Hamamatsu R4558 for an applied field of 500 mG parallel to the x axis*

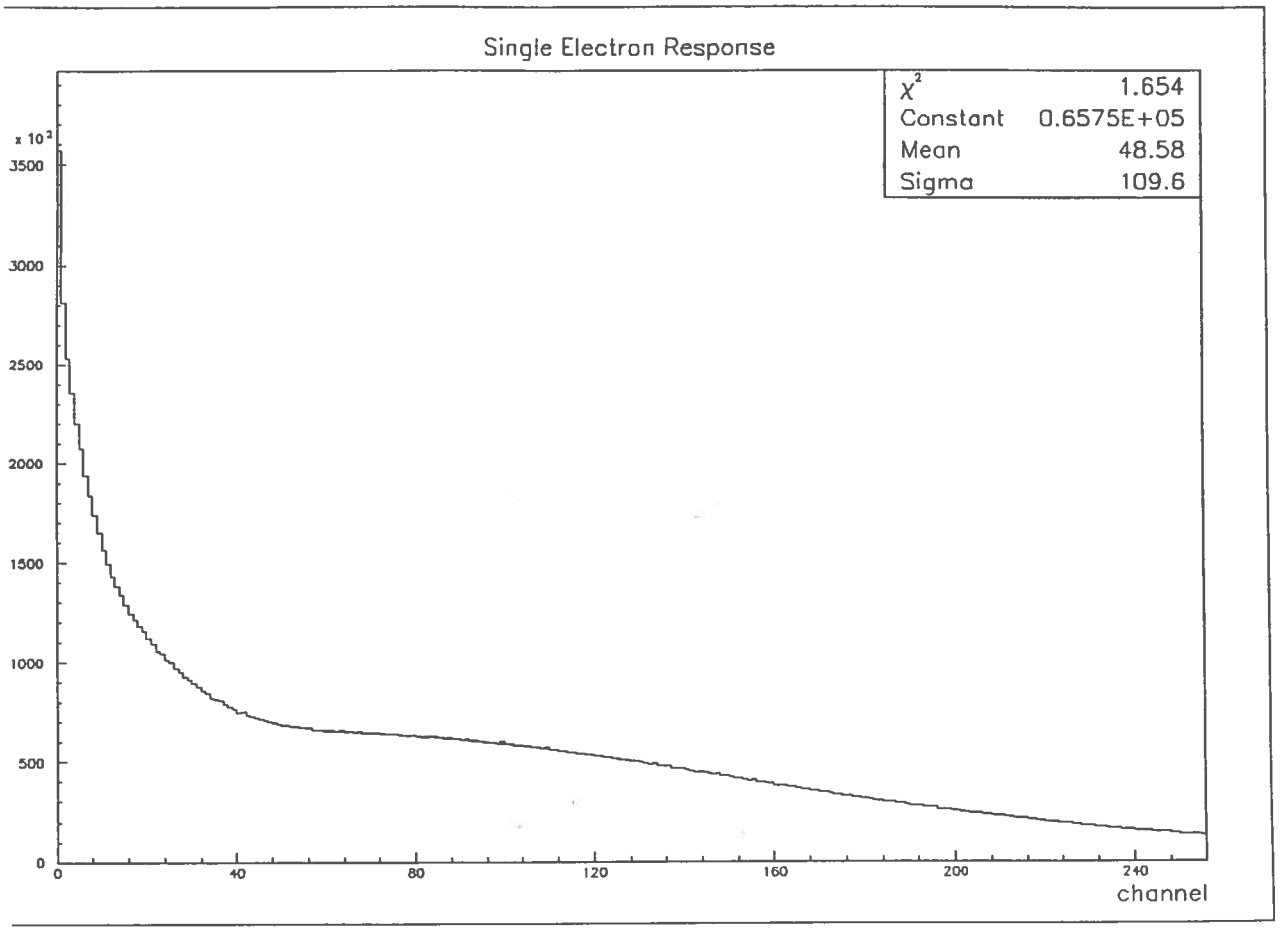


*Figure 25. Single electron response of the Hamamatsu R4558 for an applied field of 500 mG parallel to the y axis*

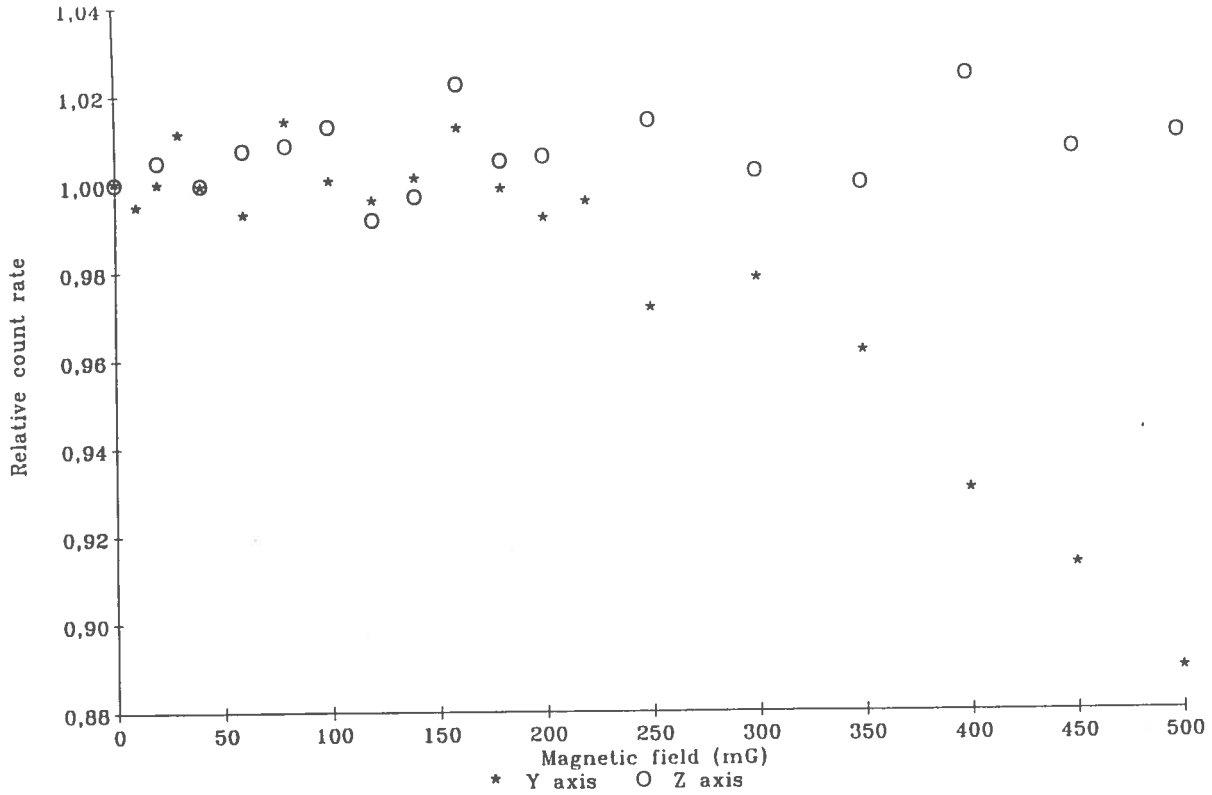


*Figure 26. Relative count rate variation as function of the applied magnetic field for the Hamamatsu R4558.*



25

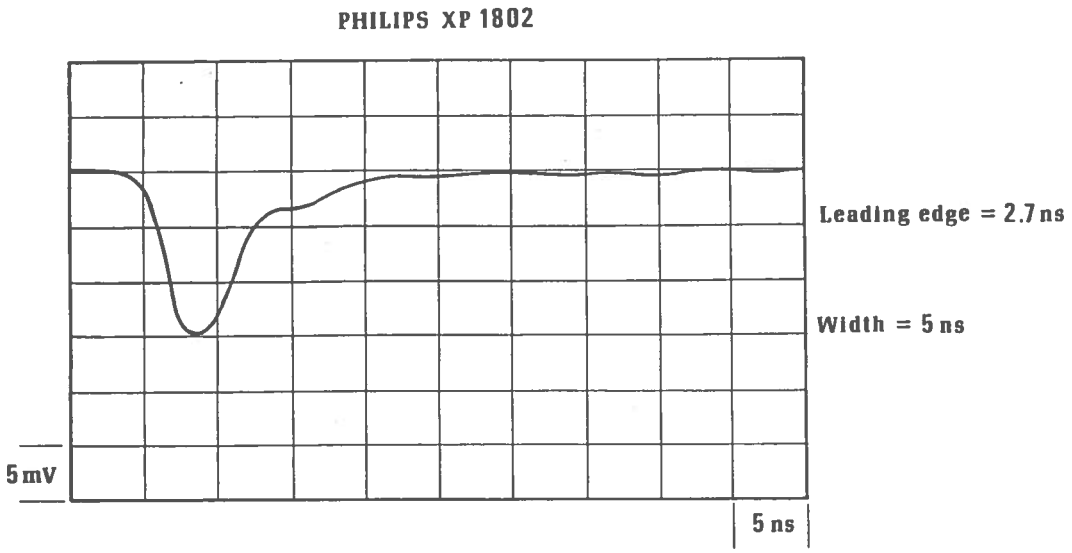


*Figure 27. Shape of the single electron anode pulse of the Philips XP1802*

## 7. - PHILIPS XP1802

### 7.1. - General features

The photocathode of the XP1802 has a radius of curvature of about 13 cm, and a minimum useful photocathode diameter of 21.6 cm, corresponding to a minimum projected area of 366 $cm^2$. The half angle subtended by the spherical photocathode is about 55 degree. The weight of the whole tube is around 1 Kg, of which 900 g is glass. Typical bialkali type (CsKSb) emissive cathode and dynode surfaces characterize this tube as well.

The linear focussed multiplier structure is provided with 11 dynodes.

### 7.2. - Anode pulse shape

The typical shape of the single electron anode pulse, obtained averaging 1000 waveforms, is reported in figure 27. The leading edge and the width values, respectively equal to 2.7 ns and 5 ns, show that this tube is very fast.

### 7.3. - Transit time spread

In figure 28 the transit time distribution measured on a sample of the tube is reported. The sigma of the best fit gaussian is around 0.9 ns, with an estimated uncertainty of 0,05 ns. The fit has been restricted only to a narrow central portion of the curve to achieve an acceptable $\chi^2$ value.

This result demonstrates the very limited dispersion of the transit time.

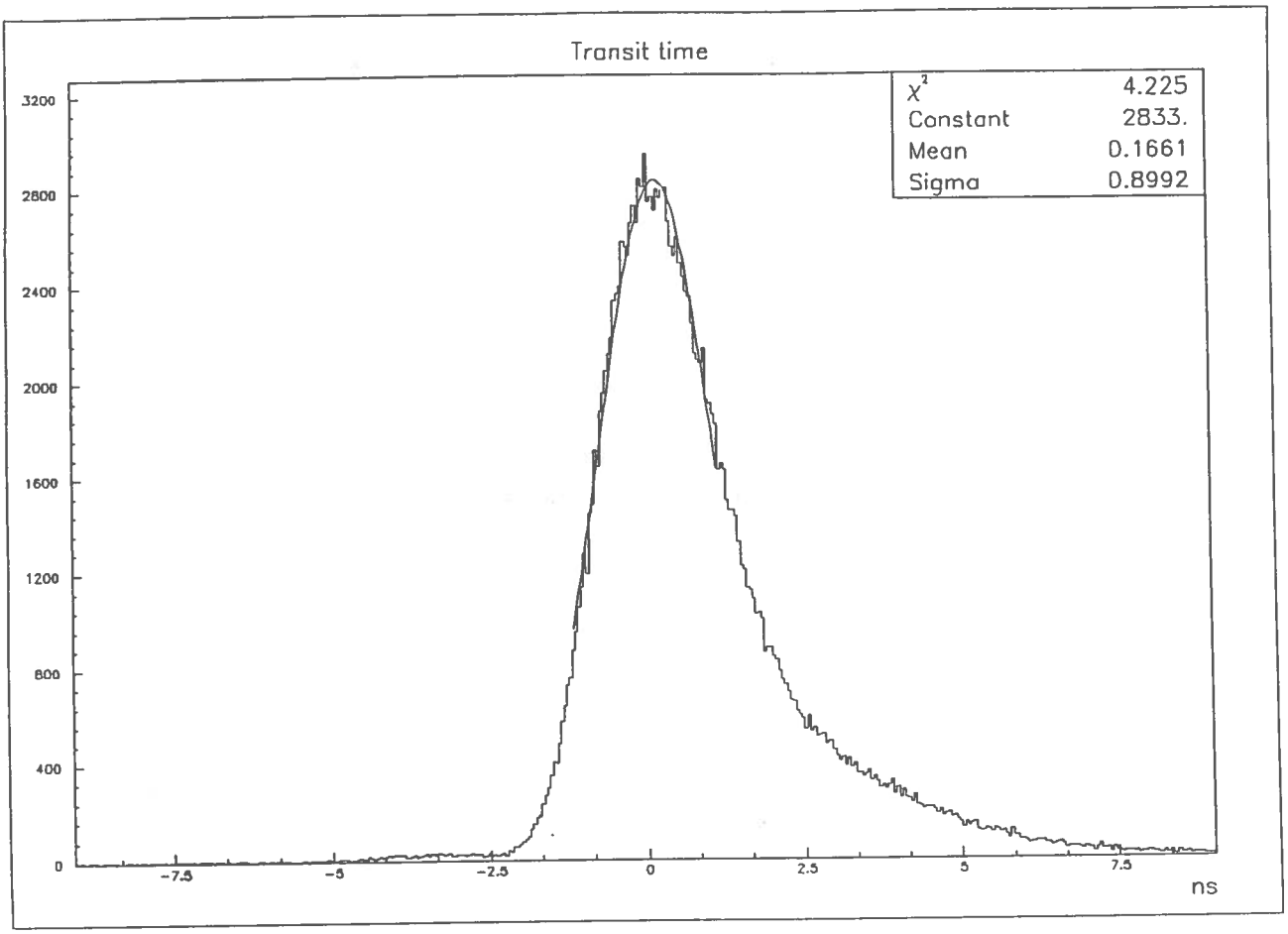


*Figure 28. Transit time distribution of the Philips XP1802*

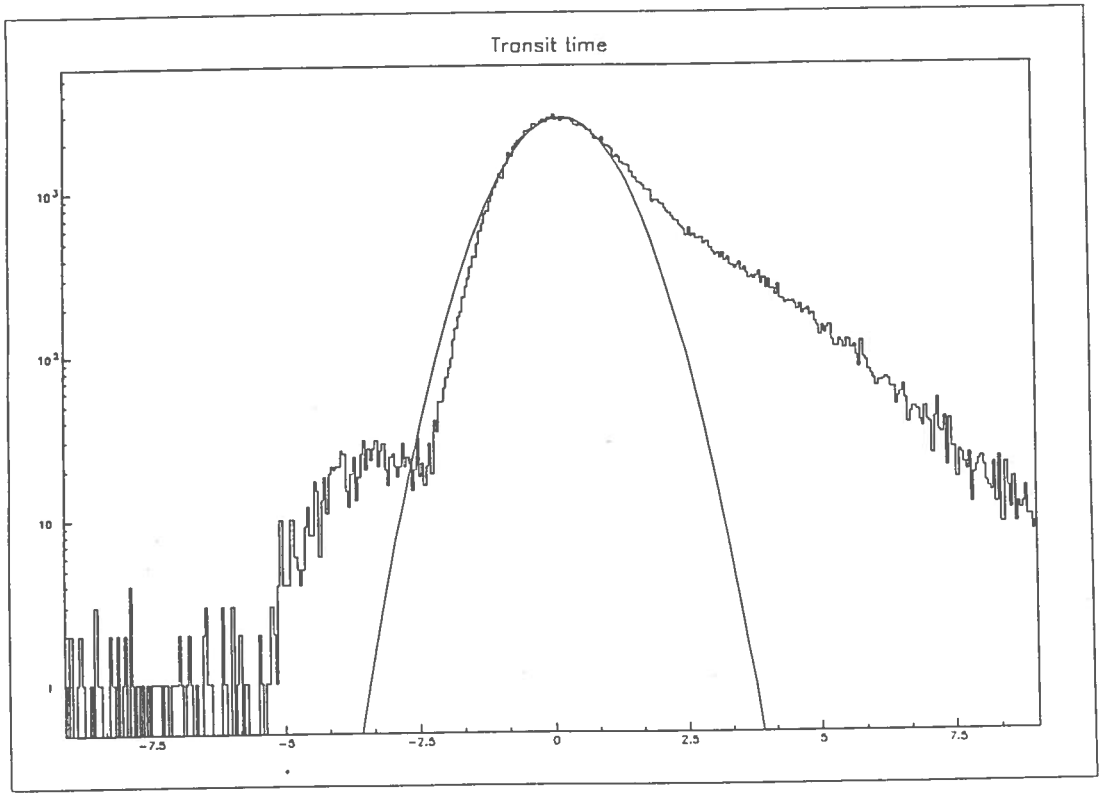


*Figure 29. Log plot of the transit time distribution of the Philips XP1802.*

## 7.4. - Pre and late pulsing

Even though the width of the transit time curve is very narrow, the figure 28 shows that the distribution is characterized by an evident tail in its right side, and by a small pre pulsing content. This effect causes a remarkable deviation from the gaussian profile, that is confirmed by the log plot reported in figure 29.

The late pulsing, defined by taking into account a 20 sigma span for the tail, is ~ 24.2%, while the pre pulsing content is only 0.5%.

## 7.5. - Afterpulses

The afterpulsing investigation was done only in the time interval from 30 ns to 100 ns, with a detection threshold of 0.1 pe. In that interval the afterpulsing probability was ~ $1.4 \pm 0.2\%$.

The measurements in the other two intervals usually considered (4 - 30 ns; 4 - 900 ns) gave the result of a very high apparent afterpulses rate, probably due to reflections in the anode output circuit following after few ns the original pulse.

## 7.6. - Dark counts and spectrum

The measurement of the dark noise rate of the tube has been performed on two samples, at ambient temperature, with a 0.2 pe threshold, and after several days of darkening. The obtained results are respectively around 1300 Hz and 1400 Hz.

The measured dark noise spectrum is reported in figures 30. It is interesting to note the clear peaked structure.

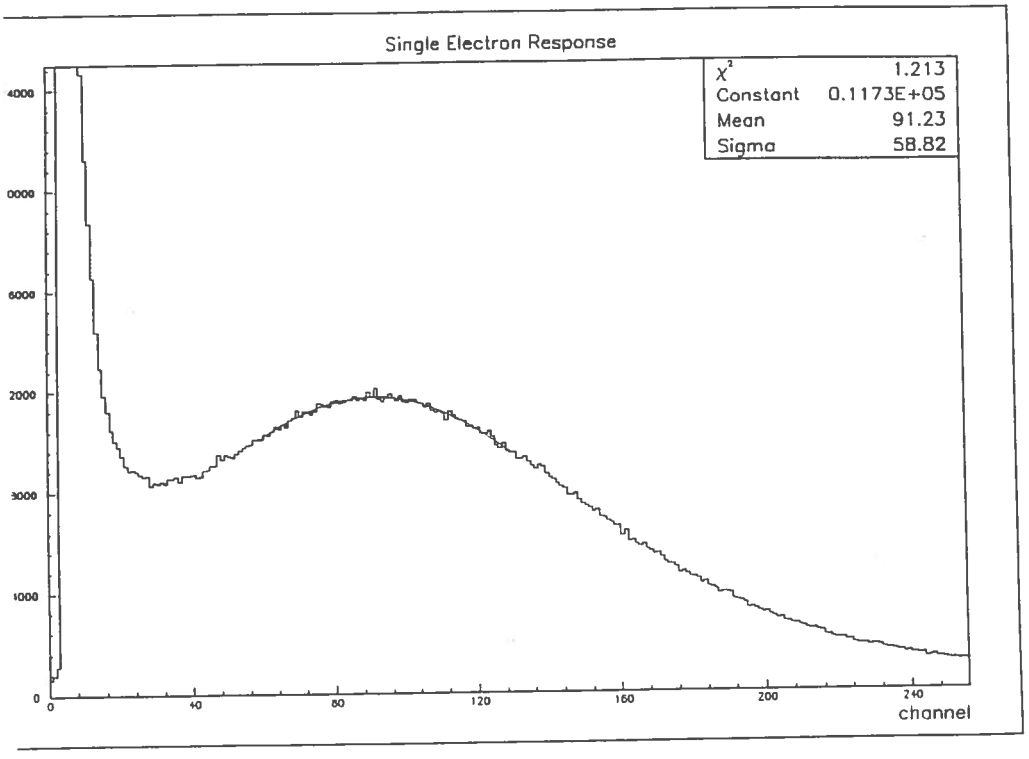


*Figure 30. Dark noise spectrum of the Philips XP1802*



28

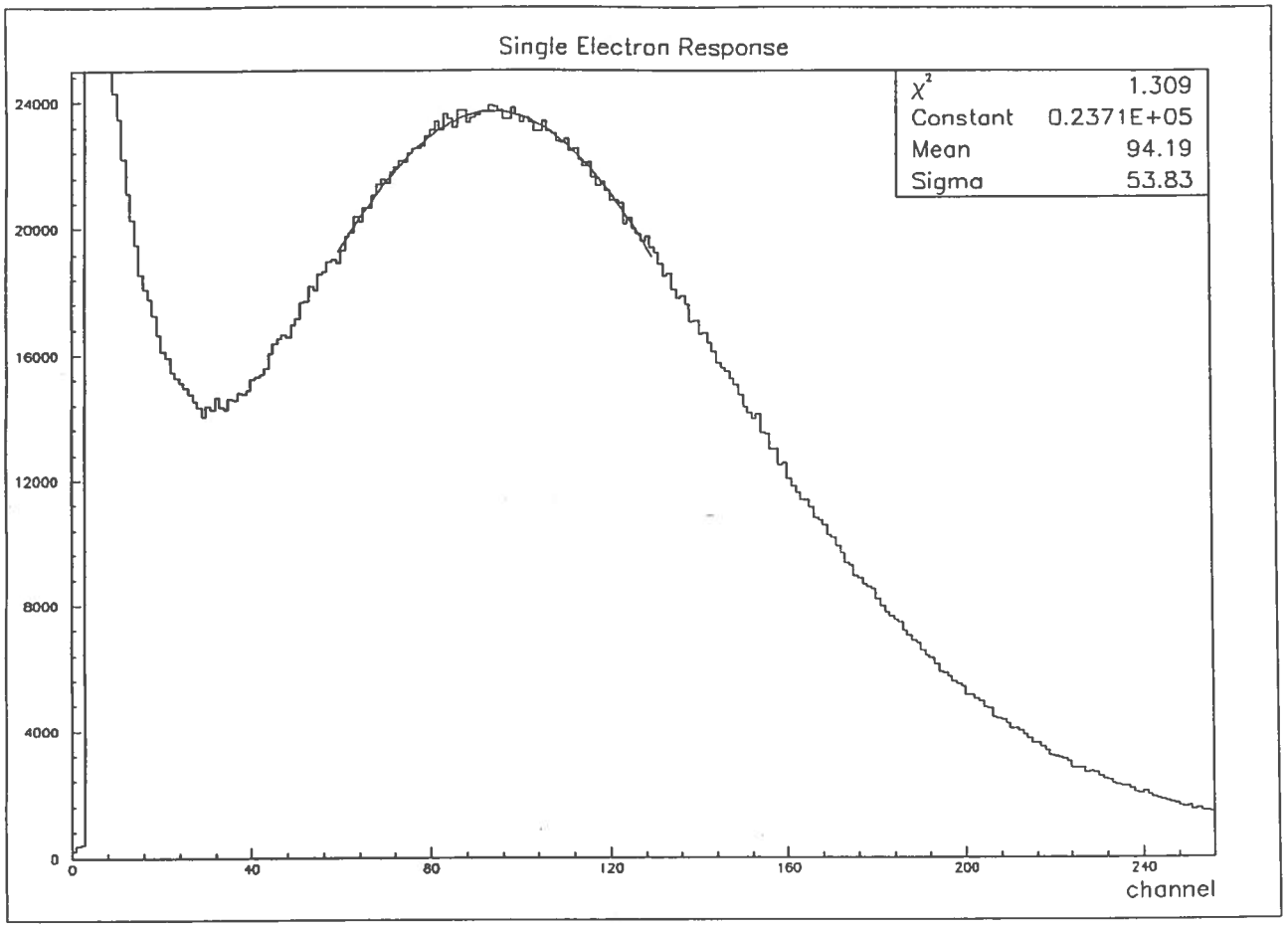


*Figure 31. Single electron response of the Philips XP1802*

## 7.7. - Single electron response

The resulting profile of the light induced spectrum is shown in figure 31.

From this figure it is possible to note that the single electron peak is more evident in this distribution than in the dark spectrum.

In detail, the peak to valley ratio and the width are 1.7 and 57.2%, respectively.

## 7.8. - Magnetic field sensitivity

The results are reported in the figures from 32 to 34, for an applied field of 500 mG parallel to the three main axis of the tube. The axis definition follows that of the Burle phototube, since the overall multiplier structure is a linear focussed one.

The results indicate that the tube is not much sensitive to the magnetic field. Indeed only a small worsening of the peak to valley ratio is visible. Only in figure 33 (y axis) not negligible displacement of the peak position is present (the lower portion of the spectrum is not visible in this figure because it was taken with the threshold set at 0.2 pe).

The single photoelectron transit time distribution for an applied field of 500 mG parallel to the x axis is reported in figure 35. The results for y and z axis are quite the same. The width of ~ 1 ns is practically unaffected by the magnetic field.

In figure 36 the count rate relative for the three axis and for field values from 0 to 500 mG is reported. No appreciable variation of the count rate is detected for the z axis, while a limited drop of less than 10% is visible for field direction parallel to the x and y axis.

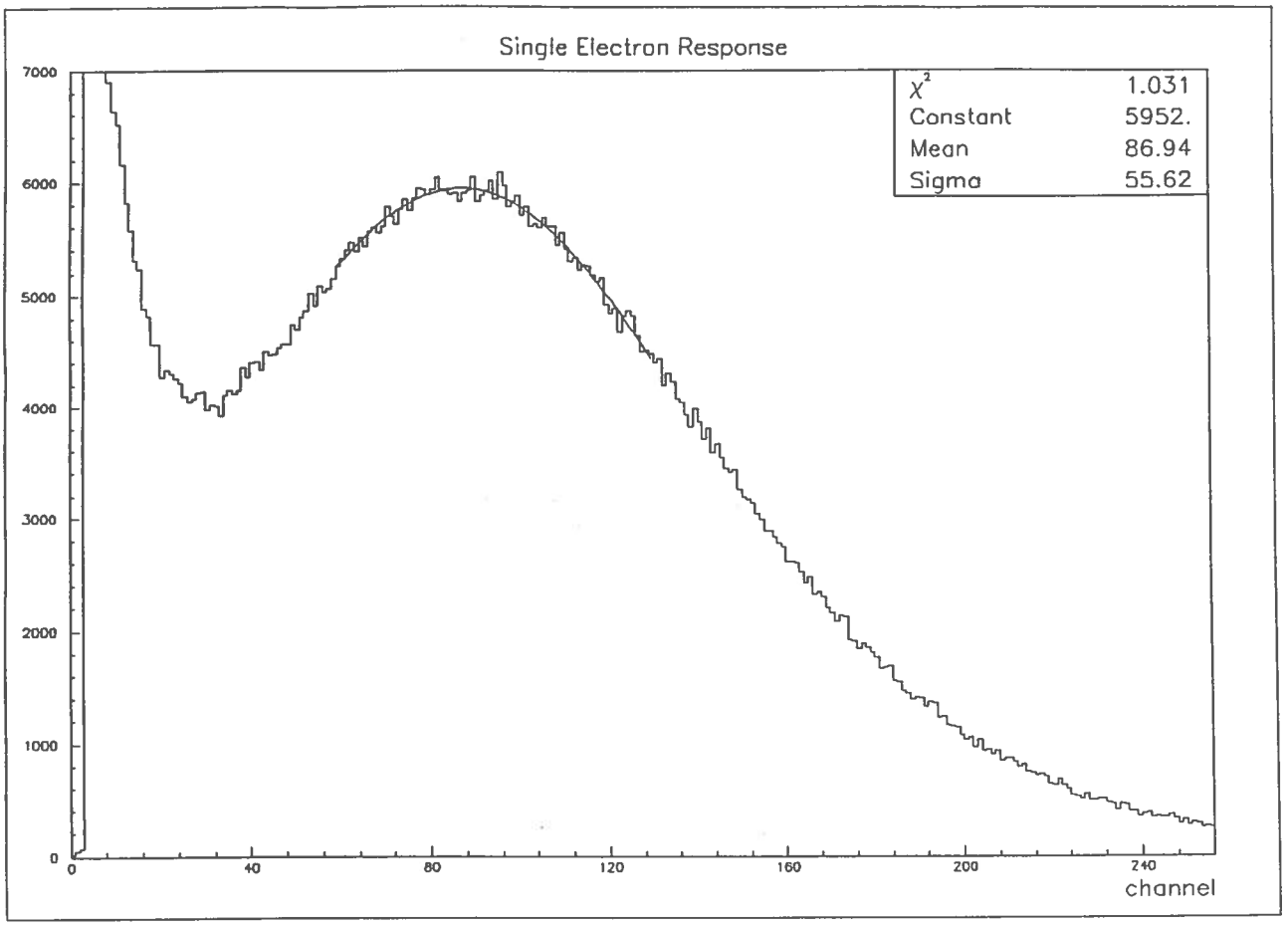


*Figure 32. Single electron response of the Philips XP1802 for an applied field of 500 mG parallel to the x axis.*

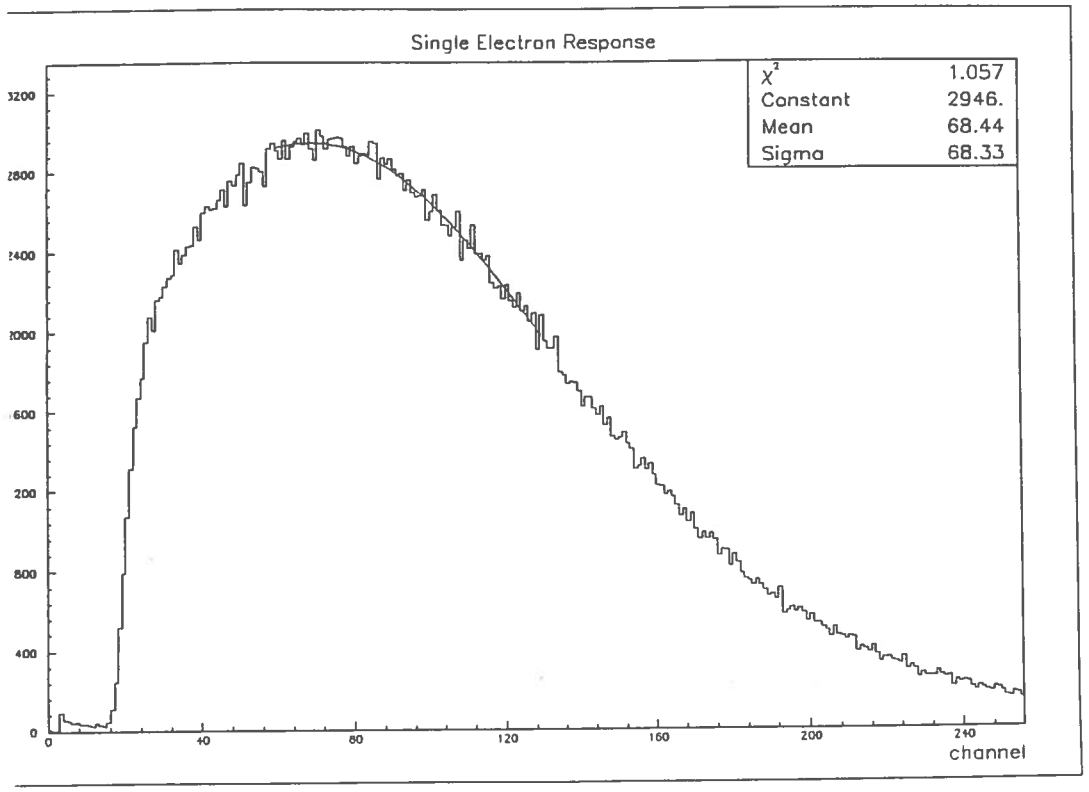


*Figure 33. Single electron response of the Philips XP1802 for an applied field of 500 mG parallel to the y axis.*

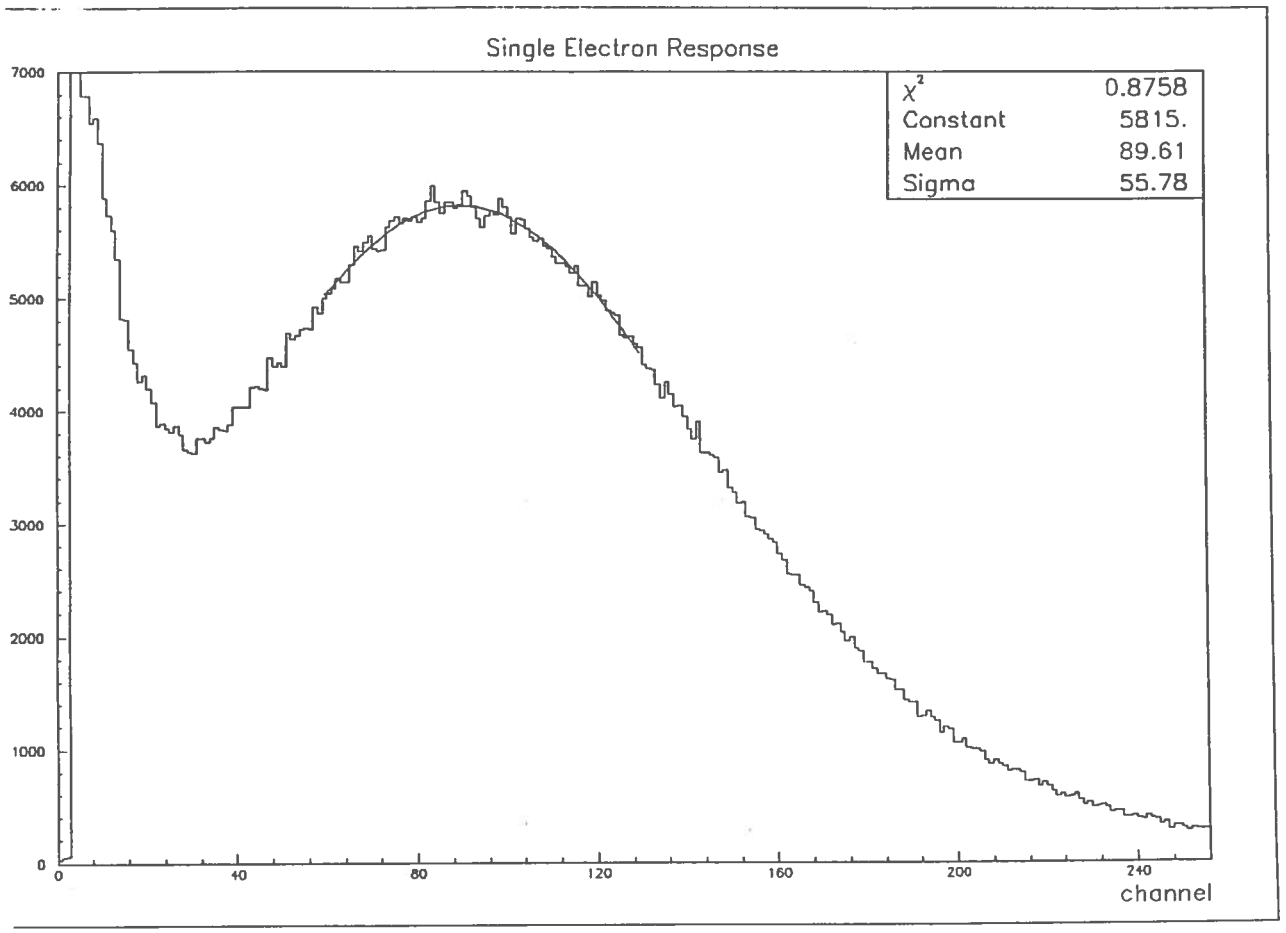


*Figure 34. Single electron response of the Philips XP1802 for an applied field of 500 mG parallel to the z axis.*

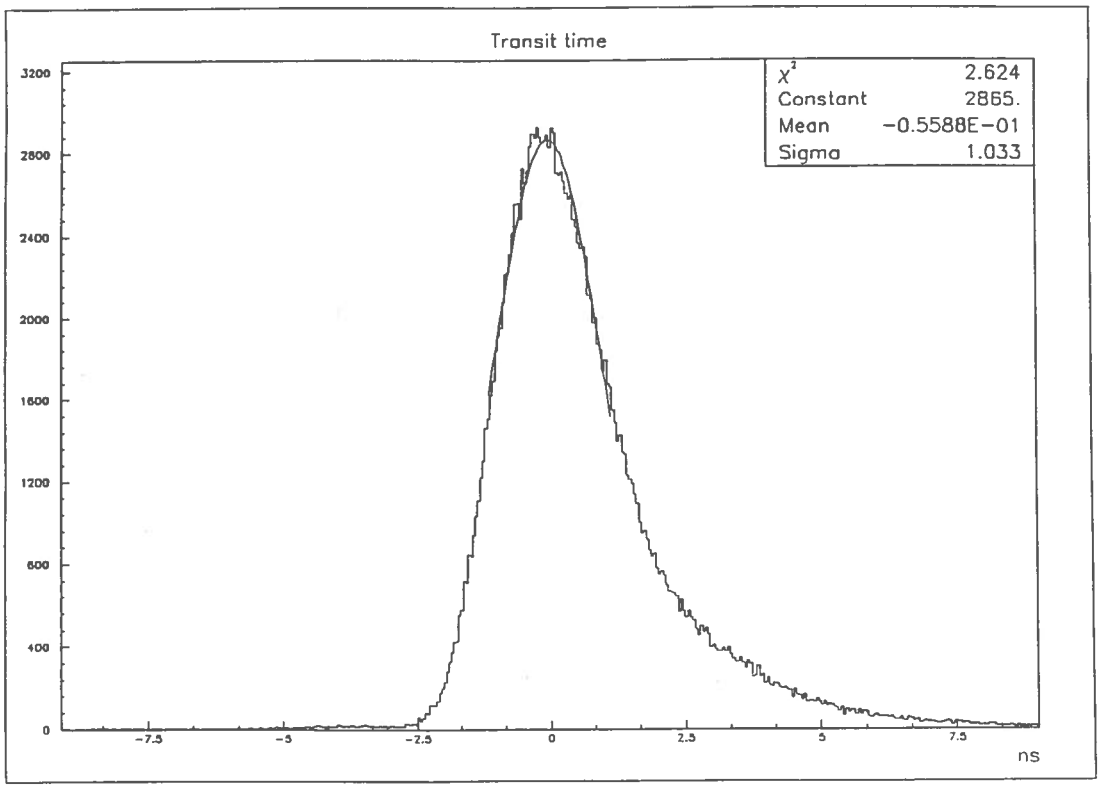


*Figure 35. Transit time distribution of the Philips XP1802 for an applied magnetic field of 500 mG parallel to the x axis.*

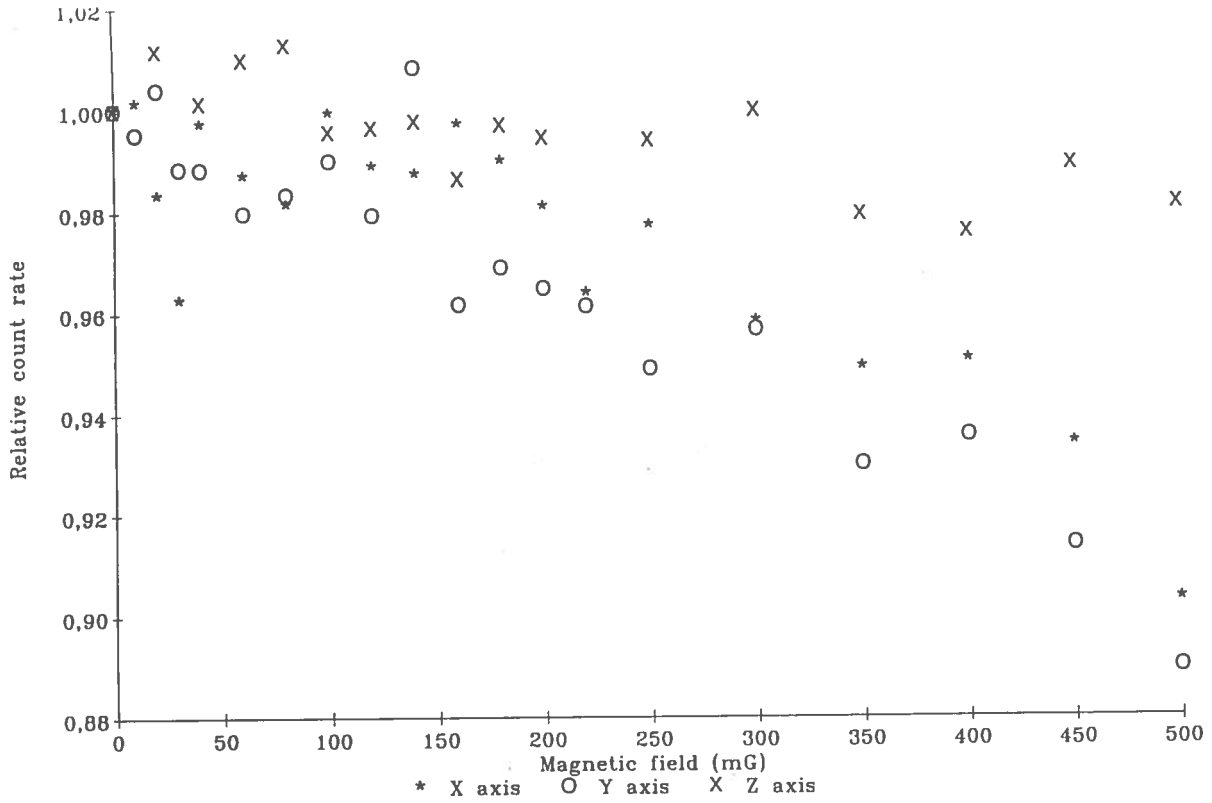


*Figure 36. Relative count rate variation for the Philips XP1802 as function of the applied magnetic field.*

## 8. - THORN EMI 9351

### 8.1. General features

The radius of curvature of the photocathode of the 9351 tube is equal to about 11 cm, with a minimum useful diameter of 19 cm, thus resulting in a minimum projected area of 366 $cm^2$. The half angle subtended by the spherical photocathode is about 72 degree. The weight of the whole tube is around 900 g, of which 800 g is glass. Also this photomultiplier is realized with bialkali type (CsKSb) emissive cathode and dynode surfaces.

The linear focussed multiplier structure consists of 12 dynodes.

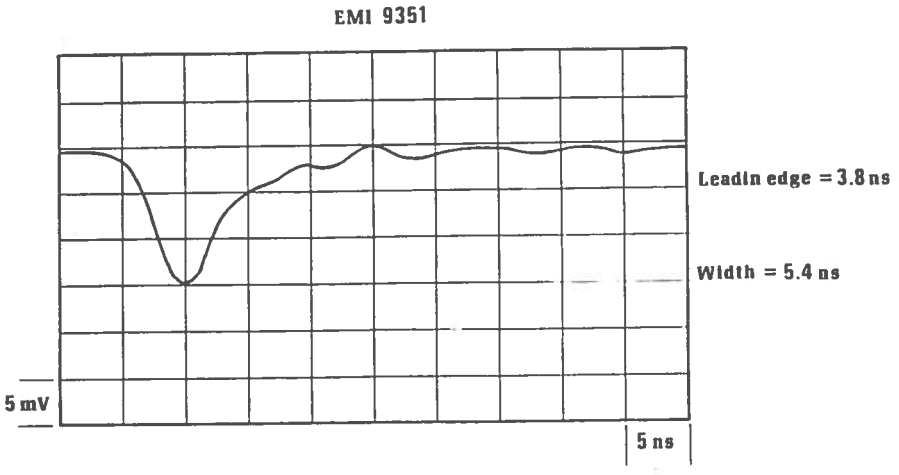


*Figure 37. Shape of the single electron anode pulse of the Thorn Emi 9351*

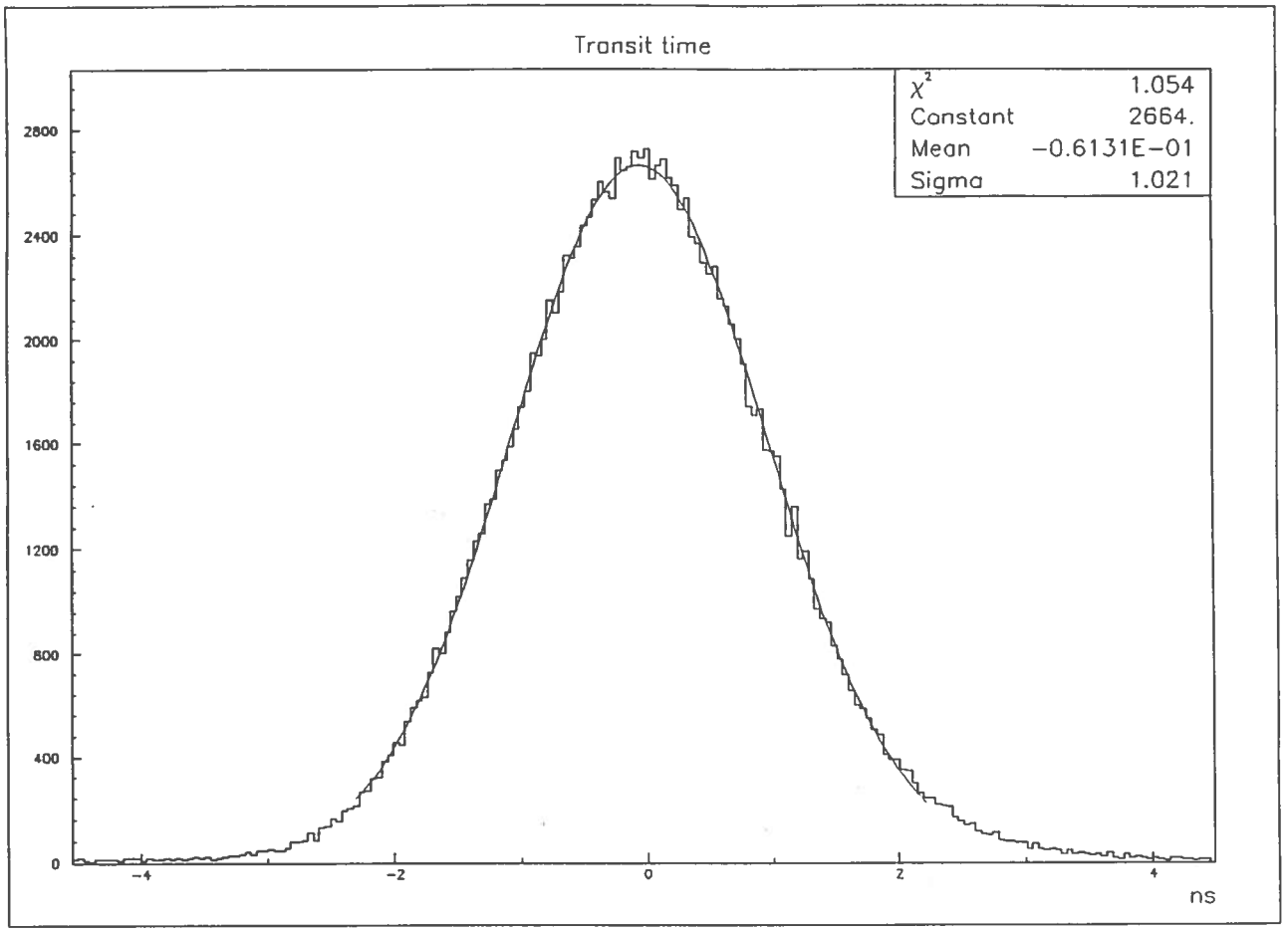


*Figure 38 Tipical transit time distribution of the Thorn Emi 9351.*

## 8.2. - Anode pulse shape

The typical profile of the single electron mean anode signal, resulting from the average of 1000 individually acquired pulses, is reported in figure 37. The leading edge and the width values, the former equal to 2.7 ns and the latter to 5 ns, point out the remarkably fast characteristic response of this photomultiplier.

## 8.3. - Transit time spread

The transit time spread measurement has been performed on three samples of the tube, obtaining very similar results. In particular in figure 38 the transit time distribution of one of them is reported. The sigma of the best fitted gaussian is practically equal to 1 ns, the estimated uncertainty on this measurements being as usual 0.05 ns. This result demonstrates the limited dispersion of the transit time typical of the tube.

It is interesting to note also the very close to 1 $\chi^2$ value, pointing out the regular gaussian like profile featured by the fitted central portion of the curve.

## 8.4. - Pre and late pulsing

The log plot of the transit time curve, reported in figure 39, on one hand confirms the regularity of the central region of the distribution, and on the other shows the tails featured both in the left and right sides. However the amount of these tails is quite limited, as indicated also by the numerical evaluation of pre and late pulsing, respectively equal to 0.5% and 1.3%.

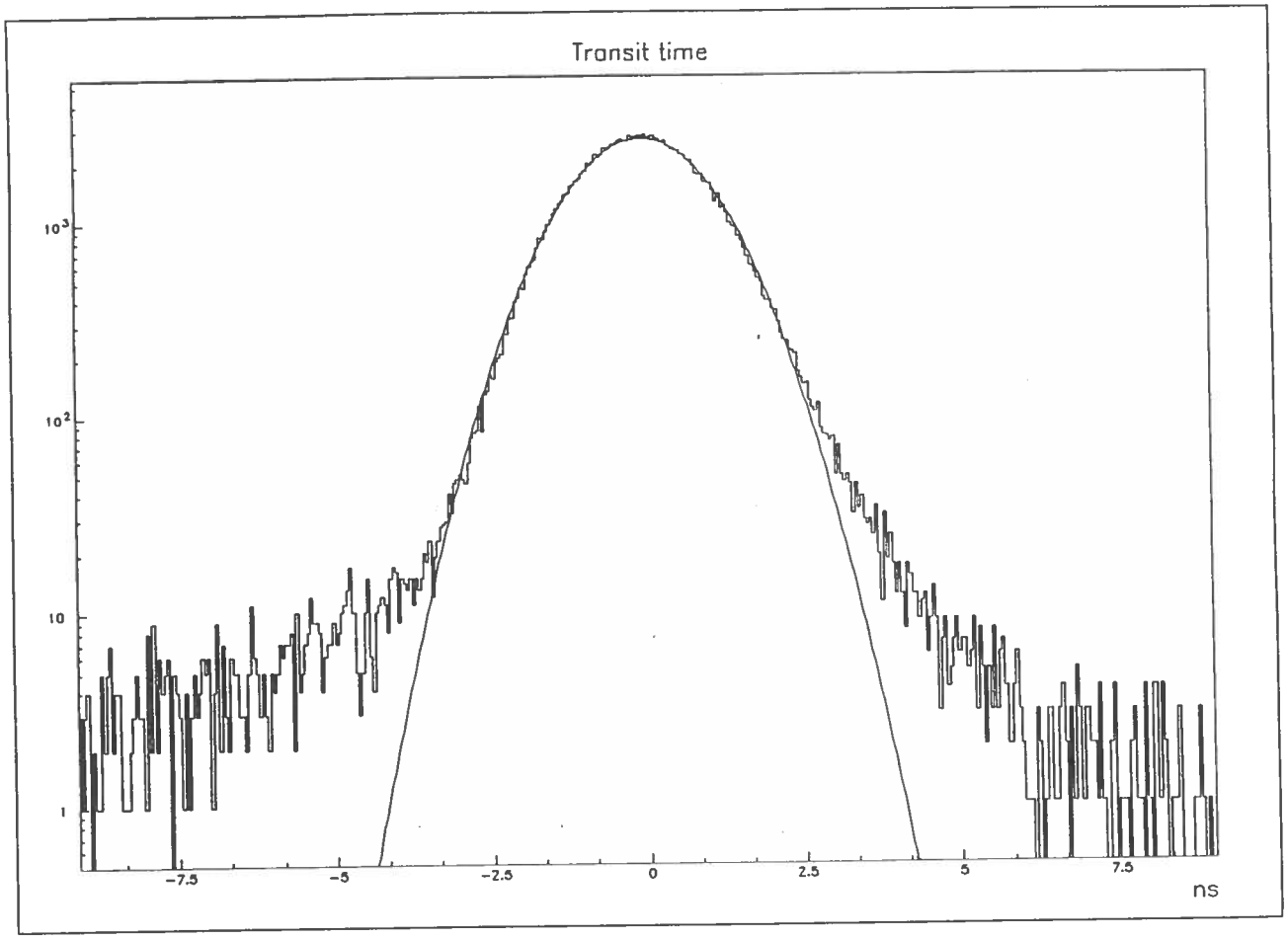


*Figure 39. Log plot of the transit time curve, enhancing the tail shape.*

## 8.5. - Afterpulses

For this tube afterpulsing investigation has been performed exploring four time intervals after the main single photolectron pulse ranging from 4 ns to 30 ns, 30 ns to 100 ns, 4 ns to 900 ns and 50 ns to 3 μs. The results, obtained as usual with a detection threshold of 0.1 pe, are reported in the table II.

*Table II - Measurements of the afterpulses for the Thorn Emi 9351*

| Time interval | 4ns - 30 ns | 30 ns - 100 ns | 4 ns - 900 ns | 50 ns - 3 μs |
|---|---|---|---|---|
| Afterpulsing prob. | 2.9 ± 0.1% | 0.15 ± 0.02% | 3 ± 0.1% | 0.4 ± 0.1% |

These measurements show the good performances of the tube regarding this parameter.

## 8.6. - Dark counts and spectrum

Dark noise measurement has been performed on two samples of the photomultiplier in the usual conditions, i.e. ambient temperature of 20°C, tube operated in complete darkness for several days, and detection threshold equal to 0.2 pe. The obtained results are remarkably low, ranging between 650 Hz and 700 Hz.

The dark noise spectrum of one of these samples is reported in figures 40. It must be noted also for this tube the quite evident peak originated by single thermoionic electrons escaping from the photocathode.

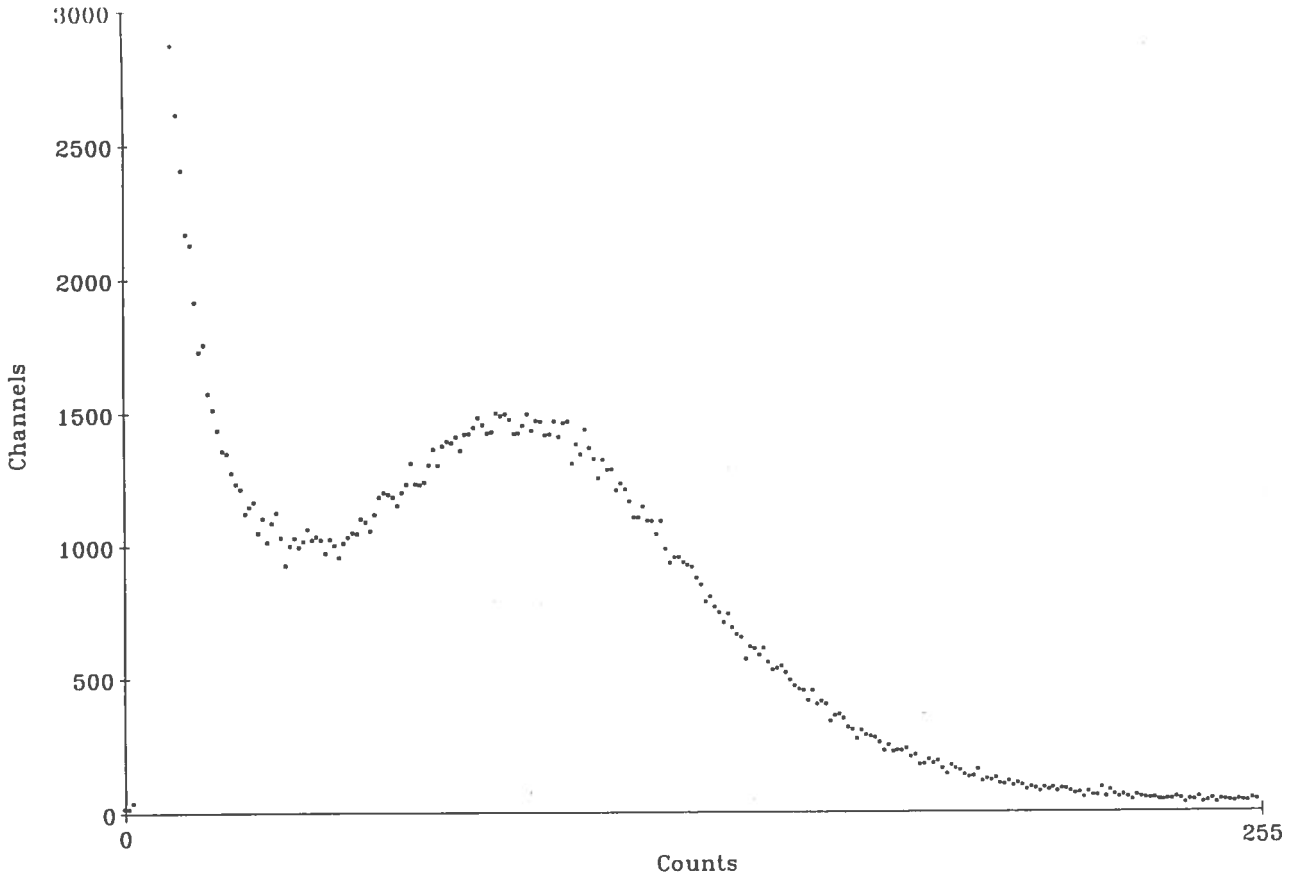


*Figure 40. Dark noise spectrum of the Thorn Emi 9351.*

## 8.7. - Single electron response

The measurement of the single electron response of three samples of the tube has demonstrated the excellent pulse height resolution of this device. This can be clearly seen from the result obtained with one of them, shown in figure 41 (the two other samples give very similar results). The peak to valley ratio and the width of this distribution are respectively 2.8 and 39.4%.

Furthermore, it is worthwhile to note how the peak featured by this distribution is significantly enhanced with respect to that in the dark spectrum.

## 8.8. - Magnetic field sensitivity

The figures 42, 43 and 44 report the single electron responses taken exposing a sample of the tube to a magnetic field of 500 mG parallel to the three main axis, whose definition is that relevant to tubes provided with a linear focussed dynode chain.

These results point out that, while for field directions parallel to the x and z axis the impact on the single electron response is practically negligible, for direction parallel to the y axis the degradation of the distribution is evident. However also in this case the curve does not lose its characteristic peaked profile.

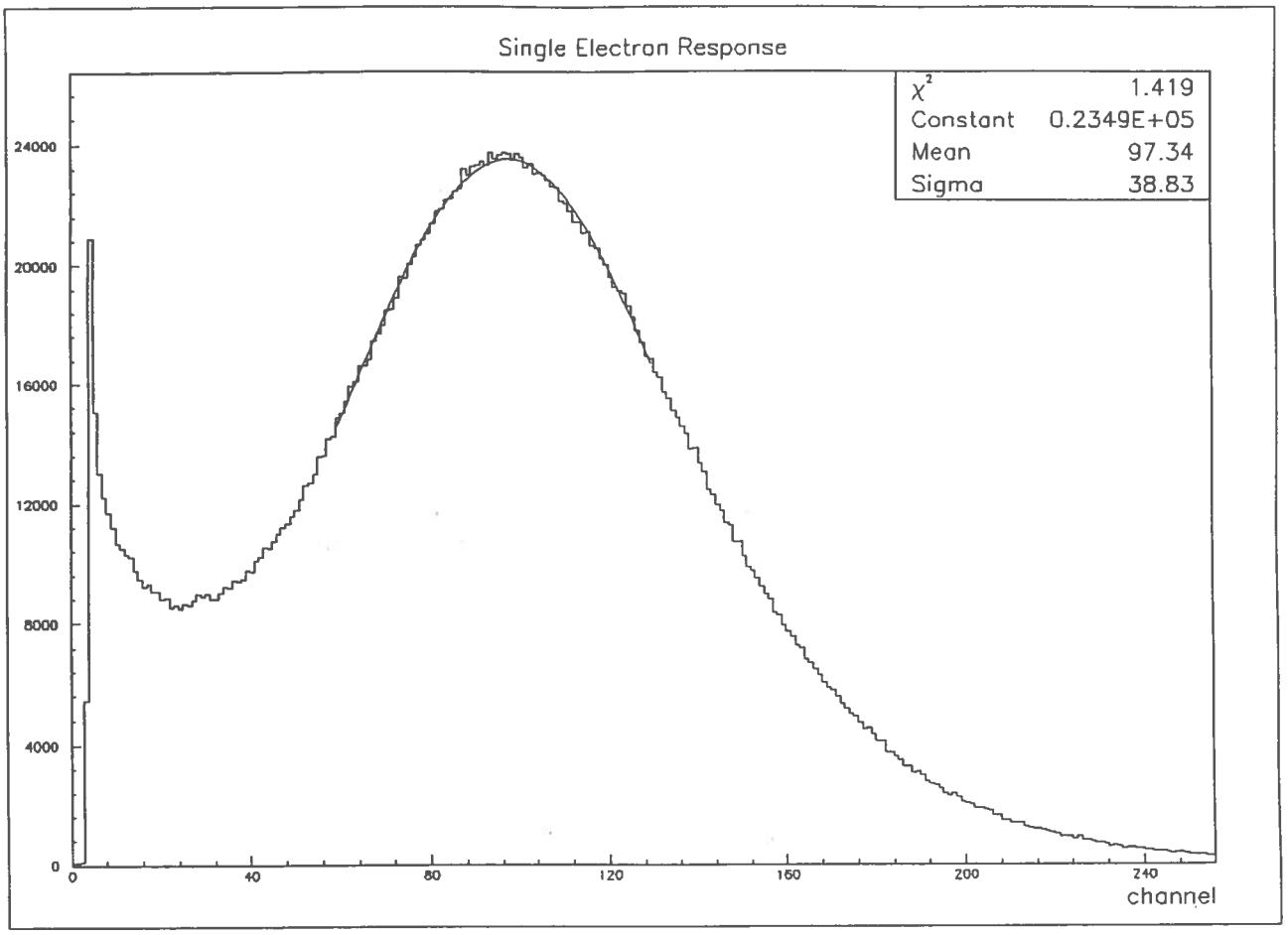


*Figure 41. Single electron response of the Thorn Emi 9351.*

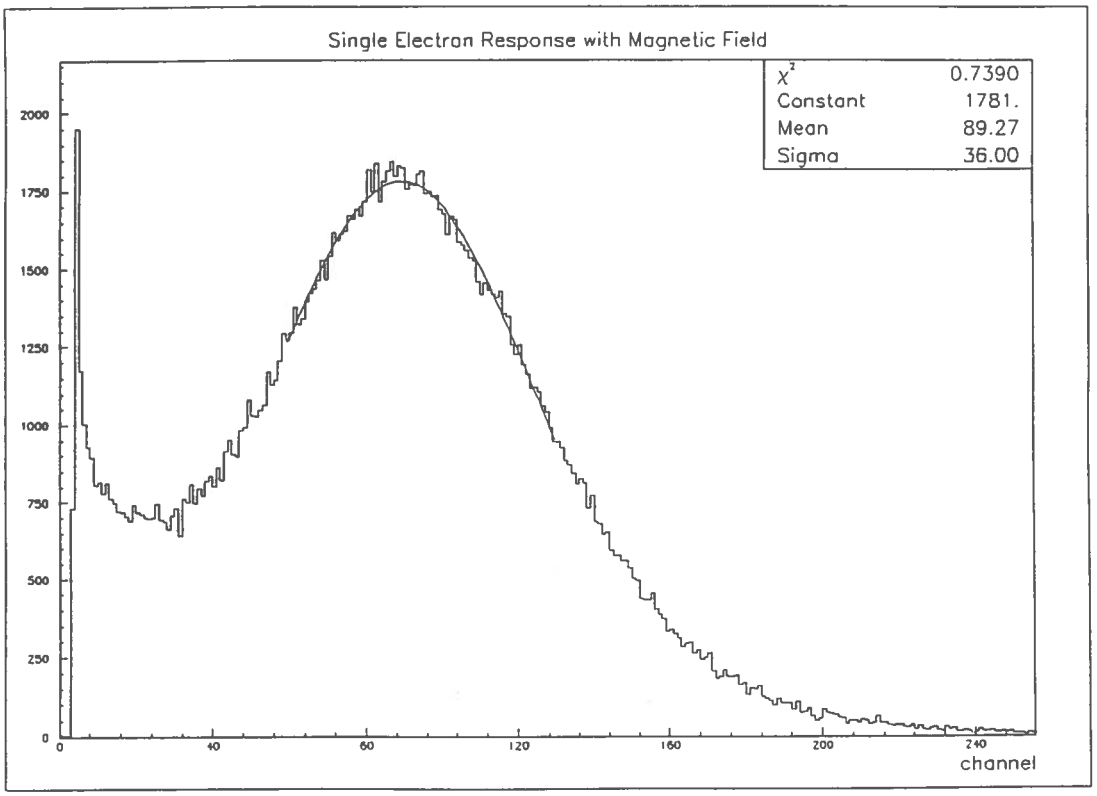


*Figure 42. Single electron response of the Thorn Emi 9351 with an applied 500 mG field parallel to the x axis*

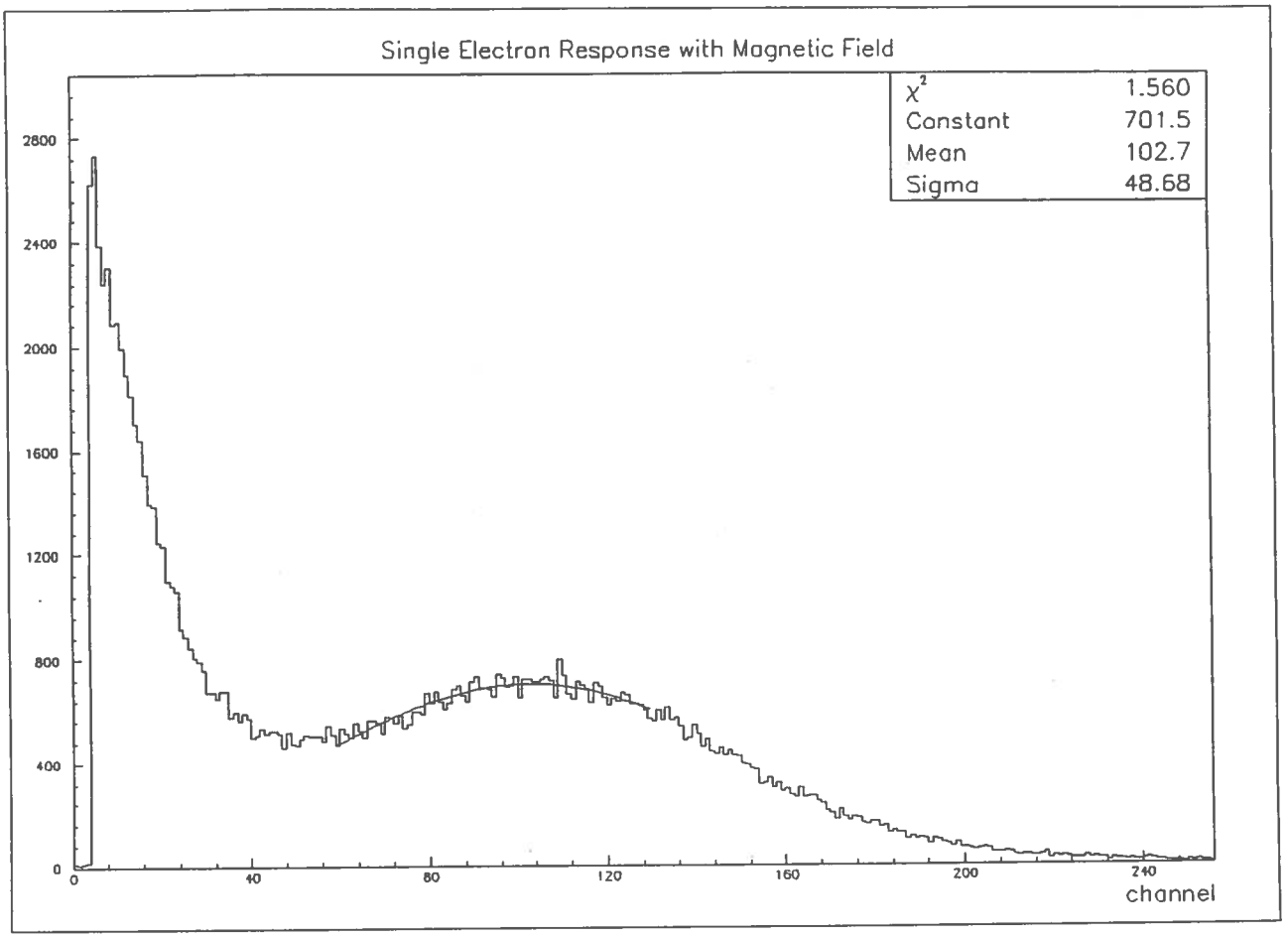


*Figure 43. As in 42 with the field parallel to the y axis.*

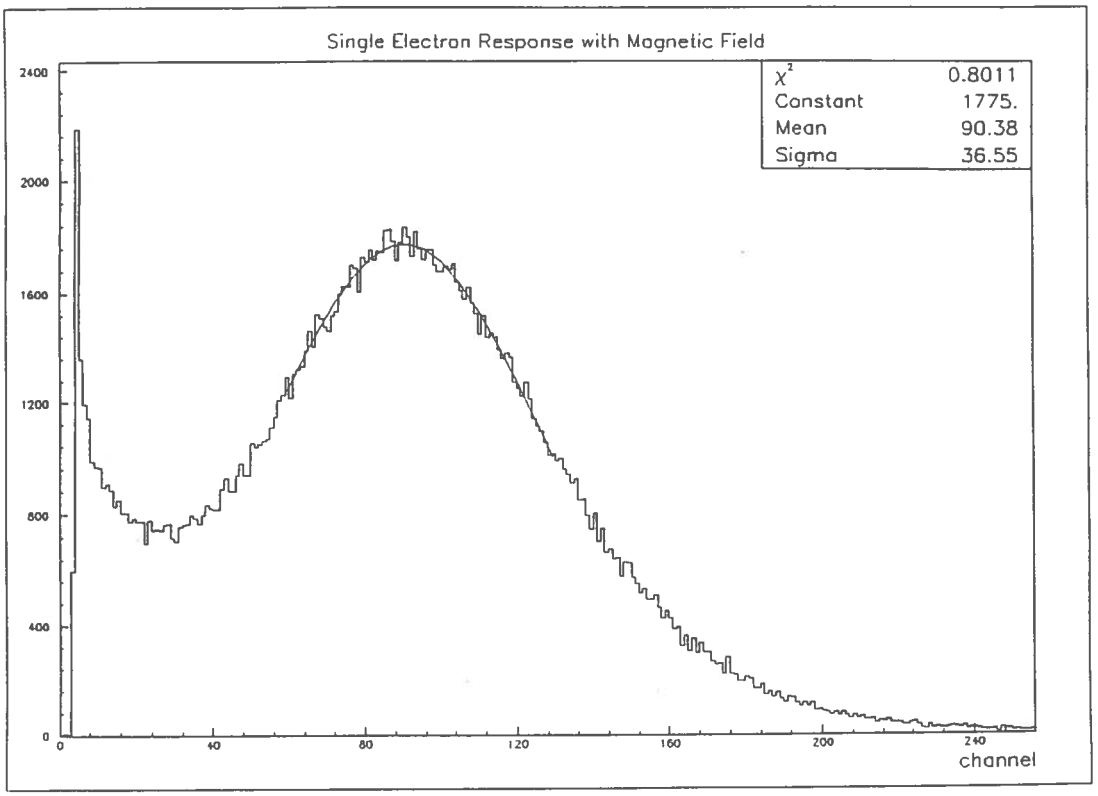


*Figure 44. As in 42 with the field parallel to the z axis.*

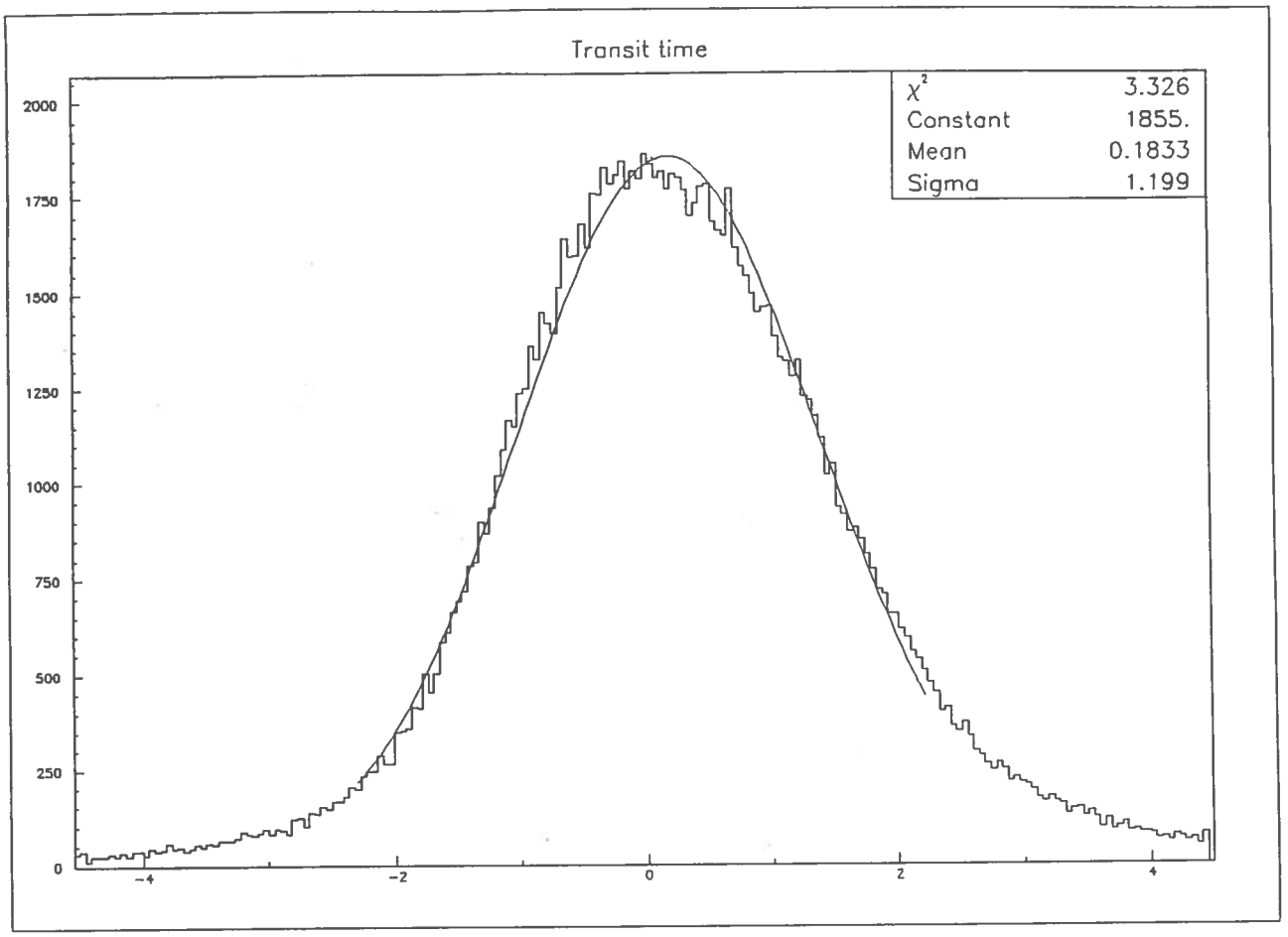


*Figure 45. Transit time distribution of the tube Thorn Emi 9351 with an external 500 mG magnetic field, parallel to the y axis.*

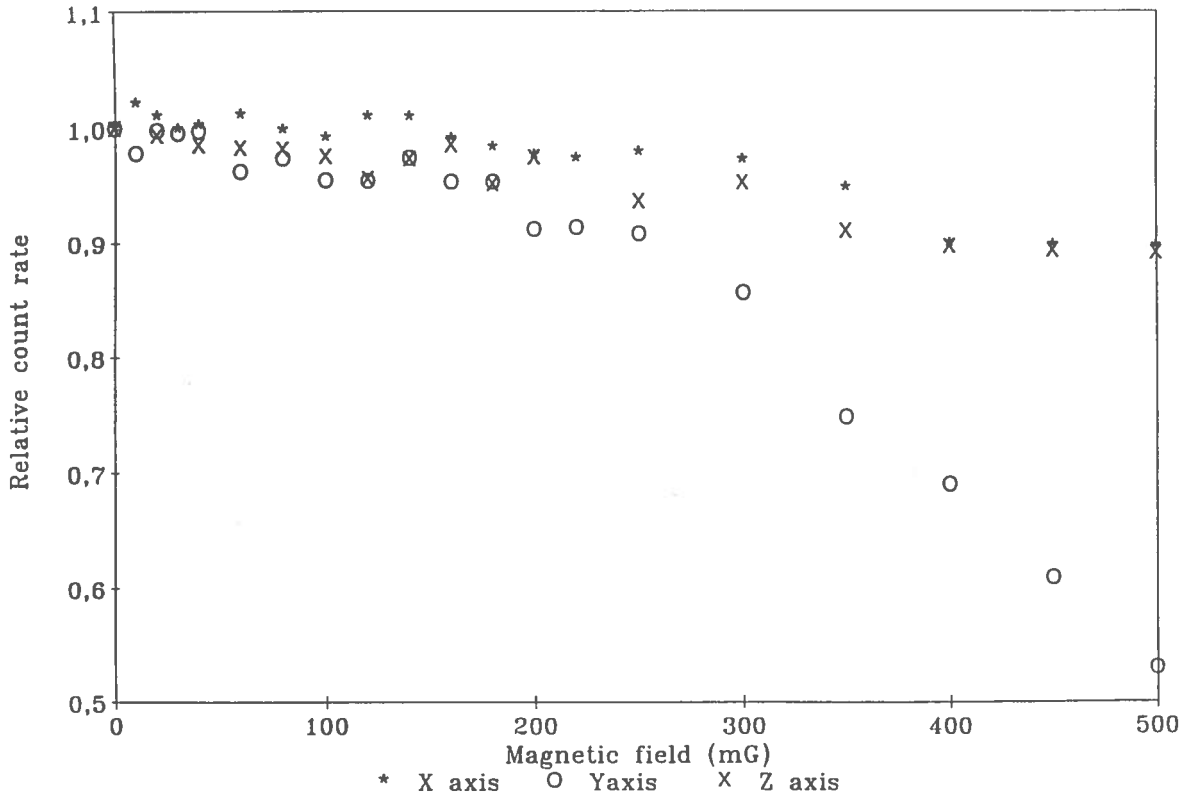


*Figure 46. Count rate variation for a magnetic field parallel to the three axis.*

Similar conclusions can be desumed from the transit time curves, measured in the same conditions as above. The curves obtained for field direction parallel to the x and z axis do not show appreciable effects. On the other hand the width of the distribution measured for field parallel to the y axis is degraded of 20%, 1.2 ns against 1 ns (with zero field); the overall shape is also distorted (see figure 45).

Finally, in figure 46 the count rate relative variations for applied fields parallel to the three axis, with values ranging from 0 to 500 mG, are reported. For the more sensitive y axis the observed variation is ~ 50%, while for the other two the count rate drop is much less pronounced.

These measurements taken together point out that the performances of the tube, even though affected by the magnetic field, however are not dramatically altered. Furhermore, they show that, for values up to 500 mG, the applied field can influence significantly the tube only if its direction is parallel to the y axis of the photomultiplier.

## 9. - HAMAMATSU 20" TUBE

Historically the first large photocathode area tube available on the market was the huge 20" R1449 photomultiplier, esplicitely developed for the Kamiokande experiment. Indeed, one thousand phototubes of this type have been successfully used over the past decade in the Kamiokande detector.

At the initial stage of the selection also this photomultiplier was considered as a possible candidate. However, it was immediately clear that the broad dispersion of the transit time, of the order of 9 - 10 ns as FWHM, and the absence of a clear single electron peak in the output anode pulse charge distribution made this tube not qualified for its use in Borexino.

Hamamatsu, in the effort of improving the properties of the tube, first realized a prototype called R1449Z, a direct evolution of the original design, characterized by a transit time spread of 7 ns, as FWHM, but still with a non visible peak, and then the totally new R3600. This last one, resulting from a completely novel design, features an evident single electron peak and a spread of the transit time limited to 5 ns, as fwhm. Although these performances are really remarkable, considering the large dimension of the tube, however the transit time spread is still to high to meet the Borexino experimental constraints.

## REFERENCES

(1) Borexino at Gran Sasso - Proposal for a real time detector for low energy solar neutrinos
Edited by : G Bellini, M. Campanella, D. Giugni
Dept. of Physics of the University of Milano
I.N.F.N. - Milano
via Celoria, 16 - 20133 Milano - Italy

R. Raghavan
AT&T Bell Laboratories Murray Hill NJ - USA



(140 pieces)